Shape From Shading as a Partially Ill-Posed Problem

J. Oliensis

COINS TR 90-50

June 1990

Shape from Shading as a Partially Ill–posed Problem [1]

J. Oliensis

Computer and Information Science
University of Massachusetts at Amherst
Amherst, MA 01003
June 13, 1990

[1]This work was supported by the Defense Advanced Research Projects Agency under grants F30602-87-C-0140 and DACA76-89-C-0017, and by the National Science Foundation under grant DCR-8500332.

Abstract

Shape from shading has traditionally been considered an ill–posed problem. However, more recently, it has been realized that the solution is strongly constrained by singular points in the image, and the belief has grown that for an image with singular points, or perhaps a visible occluding boundary, the problem in fact is well–posed. In same cases this belief is correct. In this paper, however, is presented the first analytical proof and numerical evidence that shape from shading can be an ill–posed problem *even when the image contains both singular points and the whole of the occluding boundary.* More precisely, we show that the problem can be simultaneously ill–posed *and* well–posed: although the shape corresponding to one section of an image may be well–determined or even uniquely determined, its extension in another image section may be infinitely ambiguous. These 'ill–posed' image regions are probably small fractions of the image in general. Nevertheless, they may occur frequently, in images both with and without visible occluding boundaries, and in practice may lead to instabilities and errors in shape reconstruction algorithms.

The main theoretical result of our paper answers a question which has been open since the original work of Bruss: whether the image of the occluding boundary constrains the solution to shape from shading. We show analytically that it does not. For a local image patch containing a portion of the boundary, we prove that the problem of shape reconstruction is *ill–posed.* Our proof is based on recasting the basic characteristic strip equations of Horn in a form that is completely *non–singular* on the occluding boundary. It applies to a Lambertian surface illuminated from a general light source direction.

Also, characteristic strips are given a simple interpretation as space curves. They are demonstrated to be *independent of the viewing direction*, depending only on the viewed object and the light source. Based on this result, we analyze the general structure of the image flow of characteristic strips for general light source direction. The results imply that in many cases the shape will be determined up to a small finite ambiguity over a large fraction of the image. This conclusion will be investigated further in future work.

1. Introduction

Shape from shading has traditionally been considered an ill–posed problem. However, more recently, it has been realized that the solution is strongly constrained by singular points in the image, and the belief has grown that for an image with singular points, or perhaps a visible occluding boundary, the problem in fact is well–posed [15] [7] [9]. In same cases this belief is correct [9]. In this paper, however, is presented the first analytical proof and numerical evidence that shape from shading can be an ill–posed problem *even when the image contains both singular points and the whole of the occluding boundary.* More precisely, we show that the problem can be simultaneously ill–posed *and* well–posed: although the shape corresponding to one section of an image may be well–determined or even uniquely determined, its extension in another image section may be infinitely ambiguous. These 'ill–posed' image regions are probably small fractions of the image in general. Nevertheless, they may occur frequently, in images both with and without visible occluding boundaries, and in practice may lead to instabilities and errors in shape reconstruction algorithms.

The main theoretical result of our paper answers a question which has been open since the original work of Bruss [1]: whether the image of the occluding boundary constrains the solution to shape from shading. We show analytically that it does not, confirming the earlier suggestion of Saxberg [15]. Specifically, we demonstrate that for a local image patch containing a boundary segment, the problem of shape reconstruction has an infinite number of solutions. Surprisingly, the shape solution near the occluding boundary is actually more ambiguous than it is in the neighborhood of an interior image line. The proof is based on recasting the basic characteristic strip equations of Horn in a form that is completely *non–singular* on the occluding boundary. The different solutions can then be generated simply by choosing boundary conditions on the occluding boundary itself. These results apply to a Lambertian surface illuminated from a general light source direction.

The practical implication of our results is that regions near the boundary of the image should be given less weight in reconstructing shape—ideally, shape should be reconstructed from the interior of the image outwards. Otherwise, the potential instability of the boundary shape solution may propagate errors into the central image, even if the shape in this region is actually well–determined due to singular points. Of course, noise increases the likelihood of

this occurring. The seeding of error at the image boundary when smoothness constraints are relaxed, and its propagation into the image interior, has actually been observed by Horn using a variational algorithm [5].

Apart from the special, probably small, image regions that we have identified, how well-posed is shape from shading? This question was answered previously in [9] for the case of illumination from the viewer direction, or, more generally, for a reflectance function symmetric around this direction. We showed there that for an image of a closed non-self-occluding surface without holes, in general there is essentially a *unique* shape solution. A fortiori, the problem is well-posed over the entire image, with no ill-posed regions in this case.[1]

This paper extends some of the results of [9] to the case of general illumination direction. First, we show that characteristic strips can be given a simple interpretation as space curves, and that they are *independent of the viewing direction*, depending only on the viewed object and the light source. Based on this result, the generic structure of the image flow of characteristic strips for general light source direction is analyzed. This is important because the flow of characteristic strips determines the surface solution. The result is the same as for the special illumination case studied in [9]. This, combined with the constraints on the solution provided by singular points in the image [1] [15] [9], implies that in many cases the shape will be determined up to a small finite ambiguity over a large fraction of the image. This conclusion will be investigated further in future work. If the shape solution is fairly well determined in general, then, by taking explicit advantage of the inherent constraints that determine it, one may hope to design a fast and possible reliable algorithm for recovering shape from shading [9].

2. Characteristic Strips as Surface Curves

We consider a Lambertian surface illuminated by an infinitely distant point source. The image is assumed to be formed by orthographic projection. With these assumptions, the image

[1]Note that the usual overall convex-concave ambiguity is eliminated because of our assumption that the imaged object is a closed surface—or, alternatively, by an argument from general position. This theorem holds for generic images. By definition, almost all images are generic. Those that are not can be converted into generic ones by arbitrarily small perturbations.

intensity is given by

$$I = -\hat{n} \cdot \hat{L}, \tag{1}$$

where $\hat{L}$ is the the light ray direction, and $\hat{n}$ is the surface normal. Explicitly,

$$\hat{n} \equiv \frac{(p, q, -1)}{(1 + p^2 + q^2)^{1/2}}.$$

The z direction represents as usual the depth of 3D points with respect to the image plane; p and q are the partial derivatives of z. The surface normal is defined so that it points towards the observer located at negative z.

The method of *characteristic strips* is a classical method for the solution of first–order differential equations, first applied to the shape from shading problem by Horn [3] [6]. The method is based on finding curves in the image plane along which the surface depth and orientation can be explicitly integrated. If the image plane can be filled out completely with such curves, then a complete solution for the surface has been found. These curves are computed by solving a system of differential equations. In terms of a Hamiltonian function H [9], where

$$H(x, y, p, q) \equiv I(x, y) + \hat{n} \cdot \hat{L} = 0,$$

the characteristic strip equations can be written as:

$$\dot{x} = H_p \quad (\equiv \frac{\partial H}{\partial p}), \quad \dot{y} = H_q, \quad \dot{p} = -H_x, \quad \dot{q} = -H_y. \tag{2}$$

The dot denotes a derivative with respect to 'time', an arbitrarily chosen variable that parameterizes the position along the characteristic strip. The subscripts denote partial differentiation. Explicitly,

$$\dot{x} = H_p = \frac{L_x}{(1 + p^2 + q^2)^{1/2}} - p \frac{\hat{n} \cdot \hat{L}}{(1 + p^2 + q^2)},$$

$$\dot{y} = H_q = \frac{L_y}{(1 + p^2 + q^2)^{1/2}} - q \frac{\hat{n} \cdot \hat{L}}{(1 + p^2 + q^2)}. \tag{3}$$

Also,

$$\dot{z} = p\dot{x} + q\dot{y}, \tag{4}$$

by the definition of p, q. This becomes:

$$\dot{z} = \frac{pL_x + qL_y}{(1+p^2+q^2)^{1/2}} - \hat{n}\cdot\hat{L}\frac{p^2+q^2}{(1+p^2+q^2)}$$

$$= \frac{L_z}{(1+p^2+q^2)^{1/2}} + \frac{\hat{n}\cdot\hat{L}}{(1+p^2+q^2)}. \tag{5}$$

Thus:

$$\frac{d\vec{r}}{dt} \equiv \frac{d}{dt}\begin{pmatrix} x \\ y \\ z \end{pmatrix} = \frac{1}{(1+p^2+q^2)^{1/2}}\left(\hat{L} - (\hat{n}\cdot\hat{L})\hat{n}\right). \tag{6}$$

Note our convention for the time direction: as time increases, the trajectory heads away from the light source. A curve generated by this equation is on the surface of the illuminated object, and will be referred to as a *surface strip*.

After a redefinition of the arbitrary time parameter, the equation may be rewritten as

$$\frac{d\vec{r}}{dt'} = \hat{L} - (\hat{n}\cdot\hat{L})\hat{n}. \tag{7}$$

(For simplicity, t' will be replaced by t from now on). This form makes it clear that *the surface curve corresponding to a characteristic trajectory depends only on the 3D object and the illumination direction, and not on the viewing geometry.* In other words, assuming only that the lighting is kept constant, characteristic strip trajectories in different images of an object represent the identical surface strips on the object. Also, it is clear that the surface strips can be extended smoothly beyond the illuminated region in accordance with eq. 7, so as to cover the whole of the object.

The right–hand side of eq. 7 is just $\hat{L}$ projected into the surface tangent plane. Thus *surface strips are curves of steepest ascent in the* $\hat{L}$ *direction.* In a coordinate system (not necessarily that of the viewer) where the z axis is aligned with $\hat{L}$, the x–y projection of a surface strip is a *gradient curve*, as defined in [9]: the curve in the x–y plane follows the gradient direction of the depth function z. In [9], using the fact that characteristic strips could be interpreted as gradient curves, we derived various general properties of images which were an important part of our uniqueness proof. Although this was done assuming that $\hat{L}$ was parallel to the viewer

direction, the results of this section imply that our earlier results can be easily generalized to the case of general light source direction. This is done in the next section. Below, the projections of characteristic strips into the image as 2D curves will be referred to as *image strips*.

3. Singular Points and the Flow of Characteristic Strips

The *singular points* of an image are those at which the orientation of the surface is uniquely determined. They can easily be picked out because they are maximally bright. Also, they are *fixed points* of the characteristic strip equations. At such points, the right–hand sides of the equations 2 and 7 vanish, and thus a characteristic strip originating exactly at a singular point never leaves it. In this section, we derive properties of singular points in the image, and describe the global structure of the flow of surface and image strips, generalizing the reults of [9]. Our description is valid *generically*. Thus, by definition, it is always true except for special cases which can be avoided by infinitesimal perturbations in the object shape or viewing conditions. Below, the image of the occluding boundary is referred to as the *limb*. It is always assumed to be visible in the image.

In [9] we derived the following image properties for the case of illumination symmetric around the z direction: 1) there is a finite, non–zero number of singular points in the image, 2) the Gaussian curvature of the surface at these points is non–vanishing (the singular points are hyperbolic), 3) every image strip begins and ends either at a singular point or on the limb. 2) implies that the singular points are either sources, sinks, or saddle points for the flow of image strips [14] [9], corresponding respectively to local minima, maxima, and saddle points of the depth z on the surface. We also showed: 4) there are no image strips terminating at saddle–type singular points at both ends, and 5) the number of singular points obeys the topological formula

$$N_{\mathrm{so}} + N_{\mathrm{si}} - N_{\mathrm{sad}} = 1, \tag{8}$$

where the N_{i} represent the numbers in the image of each singular point type. These properties are valid generically.

Singular points correspond to points on the object at which the surface normal is parallel to the light source direction. Thus, considered as object points, they depend only on the light

source direction, and not on the viewer. We have seen that surface strips are also independent of the viewer. Thus it is clear that many of the above results can be interpreted as direct statements about object properties, and that these properties will be manifest in images taken from essentially arbitrary directions. It is therefore fairly straightforward to generalize them to the case of illumination from an arbitrary direction. The proof involves slight modifications of the original proofs quoted in [9].

In the Appendix we prove the following theorem. Define a closed surface to be *structurally stable* if 1) the surface has a finite number of critical points of the depth function z, 2) they are non–degenerate critical points (the Gaussian curvature of the surface is non–vanishing at these points), 3) there are no surface strips connecting saddle critical points. (Note that here z is not necessarily associated with any viewer direction.) **Theorem**: 1) *Every smooth, closed surface can be approximated arbitrarily well by a structurally stable surface.* 2) *For all sufficiently small perturbations of a structurally stable surface, the perturbed surface is also structurally stable.* Thus, almost all surfaces are structurally stable. From now on, we restrict our considerations to this generic class of surfaces.

Using the theorem above, many of the arguments of [9] can be extended to apply directly to generic, 3D objects. Thus, it is easy to show that all surface strips begin and end at critical points of the depth function. Also, the index theorem argument of [9] shows that:

$$N_{\mathrm{ell}} - N_{\mathrm{sad}} = E, \tag{9}$$

where N_{ell} is the number of critical points with positive curvature (local maxima or minima of z), N_{sad} is the number of saddle critical points, and E is the Euler number of the surface. z must attain at least one global maximum and one global minimum on the surface, so $N_{\mathrm{ell}} \geq 2$. If the surface is of genus zero, i.e., a deformed sphere with no holes, then its Euler number is 2.

Let us identify the z direction with a lighting direction $\hat{L}$. Then the singular points in an image just correspond to the critical points of z on the imaged object. A local minimum of z corresponds to *a source* singular point; near these points, the direction of all surface or image strips is outwards (see e.g. [9]). Similarly, a local maximum corresponds to a *sink* singular point, with all nearby strips converging to the sink, and a saddle point to a *saddle* singular point. The concept of critical points is more general than that of singular points, since the former need not be visible in any particular image. For convenience, we will also use the terms 'source' and 'sink'

to characterize the type of a critical point on the object. Sources and sinks will be referred to collectively as *elliptical* points to distinguish them from saddle points.

Each saddle point is the originating point for two surface strips, and similarly the terminating point for two (see e.g. [9]). From the Theorem, the second two of these strips connect the saddle point to at least one, and possibly two, local minima of z (sources). Similarly, the first two connect to one or two local maxima (sinks). For genus zero surfaces, if a saddle point connects to only one source, it must connect to two sinks, and if to just one sink, then to two sources, by the Jordan separation theorem. Below, we specialize to genus zero surfaces.

Let p be a source critical point, and consider the set containing p, plus all points lying on surface strips originating at p. This set is open [9]. Let C_p denote its closure. C_p comprises either the whole of the object or else some bounded portion of it. In the first, uninteresting case, there is then exactly one source critical point p, which is the global minimum of $z(x, y)$, and one sink s, the global maximum, with no saddle points. An example is the sphere. In the second case, the boundary of C_p consists of an alternating sequence of saddle points and sinks connected together by surface strips [9]. Analogous results hold for the region of points connected to a sink s. Also, one can show that all singular points are connected to each other by sequences of surface strips [9].

All these connectivity properties will also hold for the projections of surface strips into some image plane. Let us make the standard assumption that the object is non–self–shadowing, and non–self–occluding for the chosen viewing direction. Then the above results give a simple global picture of how singular points are connected to each other by characteristic curves in the image, for general lighting direction. Let us also assume no backlighting, so that the viewer and light source are in the same hemisphere with respect to the object. Then: 1) there is a finite, non–zero number of singular points in the image, 2) the Gaussian curvature of the surface at these points is non–vanishing (the singular points are hyperbolic, and are either elliptical or saddle points), 3) every image strip begins and ends either at a singular point or on the limb, 4) there are no image strips terminating at saddle–type singular points at both ends. The index theorem result, point 5) above, does *not* generalize to the case of general light source direction, since the visible region in the image includes an unknown fraction of all critical points on the object. The description of the boundary of a source or sink region on a genus zero surface quoted above is

true in the image if the relevant image strips are visible. In the next section, it is argued that these results can tightly constrain the shape solution over much of the image.

Another important question is the behavior of image strips at the limb. We return to the coordinate system in which z is the viewing direction. Generically, the limb will be a smooth, closed curve in the image [16]. Then for points on the occluding boundary of the object, the tangent plane to the surface contains the z–direction, and also the tangent to the limb in the image plane. Thus, it is completely determined. A surface strip passing through the occluding boundary has a well–defined 3D tangent which must lie in this tangent plane. Therefore, unless this tangent has zero projection in the image plane, the corresponding image strip at the limb will be *tangent* to the limb. Moreover, as will be seen later in an explicit example, the direction of an image strip at the limb may be either into or out of the image region. This differs from the situation considered in [9]. It is another way of seeing that the index theorem result of [9] does not extend to the case of general illumination direction. It is also the basic reason why the uniqueness theorem of [9] does not extend to this case.

Lastly, we show that at the *shadow boundary*, i.e., the curve separating the illuminated from the non–illuminated region of the object, the direction of the image strips is always outwards towards the dark region. In [9], the shadow boundary coincided with the occluding boundary. It was argued there on the basis of general position that the direction of the strips is outwards at the boundary. This will remain true for general viewer direction since surface strips are independent of the viewer. A second argument is as follows: for a *closed* object that is non–self–shadowing, the surface at the shadow boundary must be 'rolling away' from the light source. Since surface strips are curves of steepest ascent in the direction away from the light source, this clearly implies that they always exit at the boundary.

The shadow boundary in the image can be distinguished from the limb, because the derivatives of the intensity are singular at the limb but finite at the shadow boundary. The fact that image strips exit only at the shadow boundary places a useful constraint on the nature of the shape solution: a singular point that is connected by an image strip to the shadow boundary cannot be a sink, for example. This type of argument was important in the uniqueness proof of [9].

4. Constraints on the Solutions to Shape from Shading

In this section, it is explained why the solutions to shape from shading may be strongly constrained in many cases. There are two reasons for this: firstly, the well–known local uniqueness results for the shape solution in the neighborhood of a singular point [1] [14] [9], and, secondly, the new, global arguments of the previous section. Our reasoning is exactly the same as in the uniqueness proof of [9]; however, for general light source direction, our conclusions are less definitive.

It was shown by Bruss [1], for the case of illumination from the viewer direction, that there is a unique local solution in the neighborhood of a singular point p which is convex at p (p is a source for this solution), and a unique local solution which is concave at p (with p a sink). Saxberg [15] noted that these results were also true for general illumination direction. Recall that if the surface solution is known at some image point, then it can be computed as well along an image strip starting from that point. Thus, the 'local' concave or convex solution can actually be extended over the whole region of points connected by image strips to the original elliptical point. So if the sources and sinks can be identified in the image, then the surface can be computed over the regions connected to these points—at least up to unknown translations in depth, since the relative depths of the singular points may not be known. Moreover, from the previous section, almost every object point is connected by a surface strip to an elliptical critical point. In many cases, therefore, a large fraction of the image may be visibly connected to elliptical points, determining the surface over this part of the image.

We also noted in the previous section that all critical points are connected to each other by sequences of surface strips. In the image, therefore, many of the elliptical singular points may be connected by sequences of image strips. If so, the relative depths of the connected singular points are determined, and the relative depths of all points connected to them as well. Thus, it may be possible to eliminate some of the ambiguity mentioned above in the relative depths of different singular point regions.

It can also be possible to determine which singular points are of which type. Firstly, not every singular point can be consistently interpreted as elliptical. Suppose a singular point p is interpreted as a source. One can solve for the characteristic strips emanating from p under

this assumption. These strips are not allowed to intersect with each other in the image [9]. If they do, then the original source interpretation was incorrect, and the singular point must be of saddle type. (It cannot be a sink, since sink image strips differ from the source interpretation only in their direction.) It is likely that many saddle points can be identified in this way.

Also, if a source or sink connects via an image strip to another singular point, then the type of that singular point is specified uniquely [9], according to the nature of the flow of strips joining the two. Moreover, if a given singular point is known or guessed to be elliptical, then it can fix by a chain reaction the types of singular points connected to it indirectly by sequences of image strips.

Lastly, the shadow boundary can be used to determined the type of singular points as described in the last section. For all these reasons, therefore, the ambiguity in the choice of singular point type may not be great. In many cases, the surface solution may be well determined up to a small, finite ambiguity over a large fraction of the image—or even uniquely determined.

On the other hand, we show by example in section 6 that there can be regions in the image which are governed by no visible singular point. The points in these regions lie on strips which are not *wholly* visible in the image, and therefore are not connected at least visibly to elliptical points in the image. These regions abut the limb, but this imposes no constraint on the corresponding shape solution by the arguments of section 5. They are therefore unconstrained, and in general the shape solution is expected to be ambiguous for these regions. This is demonstrated numerically in section 6 for one of the examples. For the specified region, shape from shading is an ill–posed problem.

Unconstrained regions of the type we discuss in section 6 occur whenever a surface strip from a visible, elliptical, singular point reenters the visible region after exiting it. The boundary of such a region is given by the first strip that does not actually leave the visible region, i.e., it is tangent to the image boundary at some point, but continues in the visible region until it finally exits somewhere else. As demonstrated by the example, this can occur for quite simple shapes, and a range of viewing conditions. However, since the surface strips are curves of steepest ascent in the light ray direction, in order for the occluding boundary to intersect one twice it must also be ascending rapidly—in fact, more quickly than the surface strip over some interval. For many

objects, the occluding boundary probably does not ascend sharply in the $\hat{L}$ direction for very long. Thus, one might expect that the unconstrained regions will tend to be small fractions of the image.

There are certainly other types of image regions for which shape from shading may be ill–posed. For instance, consider a three–sided region, bounded by the limb and two of the strips connecting to a saddle singular point, and assume it contains no interior singular point. An example of such a region is given in section 7. The existence of such regions has also been noticed by Saxberg [13]. This region is constrained only by the saddle singular point. It has not yet been established whether, for general light source direction, a saddle point can constrain the shape solution in its neighborhood. If it does not, then shape from shading is probably ill–posed in this region type.

In all of the examples that have been considered so far, the shape solution is well–determined over most of the image, and ill–posed only for a small fraction of the image. Further experiments will investigate the extent to which this holds true in general.

5. Shape Reconstruction near the Limb

In this section, the characteristic strip equations near the limb are examined, and it is shown that the limb does not constrain the shading solution. This is the main theoretical result of the paper. The difficulty in doing this stems from the singularity of the variables p and/or q at the limb. Thus we begin by rewriting the equations in a rotated coordinate system, in terms of variables that remain finite on the limb. This strategy of using a rotated coordinate system has also been explored by Saxberg [15].

The characteristic strip equations are eq. 7 above and:

$$\dot{p} = -\frac{\partial I}{\partial x}(1 + p^2 + q^2)^{1/2}, \qquad \dot{q} = -\frac{\partial I}{\partial y}(1 + p^2 + q^2)^{1/2}, \tag{10}$$

with the surface represented by $z(x, y)$, p, q. Instead, we switch to representing the surface by a function $y(x, z)$, and y_x, y_z, which should be possible at least locally. These quantities indeed remain finite on the limb.

Define the variables

$$w \equiv -\frac{p}{q}, \qquad v \equiv \frac{1}{q}. \tag{11}$$

If a surface solution $y(x,z)$ exists, then $w = y_x$ and $v = y_z$. These variable evolve via:

$$\dot{w} = \frac{-\dot{p}}{q} + \frac{p\dot{q}}{q^2} = \frac{v}{|v|}(I_x + wI_y)(1 + w^2 + v^2)^{1/2},$$

$$\dot{v} = -\frac{\dot{q}}{q^2} = \frac{v}{|v|}(vI_y)(1 + w^2 + v^2)^{1/2}. \tag{12}$$

The existence of a surface solution $y(x,z)$ also implies that

$$I_x \equiv \left.\frac{\partial I}{\partial x}\right|_z = I_x + y_x I_y, \qquad I_z \equiv \left.\frac{\partial I}{\partial z}\right|_x = y_z I_y, \tag{13}$$

where on the left-hand side $I(x, y = y(x,z))$ is thought of as a function of x, z. Although I_x or I_y must be singular on the limb, I_x and I_z are both *finite*. The equations 12 appear to have almost the same form in the rotated coordinated system as they did in the original one, with y playing the role of z.

At least one surface solution of the characteristic strip equations can be assumed to exist—namely the original object from which the intensity image was derived. The basic strategy of our proof is to write the equations with reference to this "pre-existing" solution. Below, therefore, y_x and y_z denote the partial derivatives corresponding to this reference solution. Similarly, I_x^r and I_z^r denote the partial derivatives of the intensity assuming the reference solution. These quantities should be thought of as fixed functions of x and y, like the intensity I itself. They have the nice property that they remain finite on the limb.

One has:

$$I_y = \frac{I_z^r}{y_z}, \qquad I_x = I_x^r - I_z^r \frac{y_x}{y_z}. \tag{14}$$

Substituting into the eqs. 12 yields:

$$\dot{w} = \mathrm{sign}(v)(I_x^r + I_z^r \frac{w - y_x}{y_z})(1 + w^2 + v^2)^{1/2},$$

$$\dot{v} = \mathrm{sign}(v) v \frac{I_z^r}{y_z}(1 + w^2 + v^2)^{1/2}. \tag{15}$$

The surface normal can be written as:

$$\hat{n} = \text{sign}(v)\frac{(-w, 1, -v)}{(1 + w^2 + v^2)^{1/2}}. \tag{16}$$

Since $\hat{n}$ is expressed as a function of w and v, the system of equations 7 and 15 form a complete set that can be solved for x, y, z, w, v as functions of time. For the reference solution, the surface normal n_z^r has the same form as eq. 16 with $(v,\ w)$ replaced by $(y_z,\ y_x)$. Since the limb is defined by $n_z^r = 0$, it follows that $y_z = 0$ on the limb, and only on the limb. The singularity of the equations 15 is due solely to this vanishing of y_z.

What is the significance of this singularity? To answer this question, we consider the signs of the various quantities in the above equations. Let us restrict our considerations to a small portion of the image bordering the limb. Image plane coordinates are chosen so that the limb is tangent to the x direction at some point; this point can be taken to be the origin. For convenience, we assume that y attains a local maximum at this point, so that the limb is convex there. Also, it is assumed that the reference surface is 'rolling away' at the limb. The opposite assumption, with the limb representing an edge projecting towards the viewer, would violate general position [9], and is impossible for a closed surface.

In the evolution equation for v, the variation of v is proportional to v itself. Thus v never changes sign except at singularity points of the right–hand side, namely on the limb. Therefore, v and y_z can be chosen positive over the given region, and the sign factors in eqs. 15 and in $\hat{n}$ can be neglected. Henceforth, we will drop the sign factors from these equations.

The sign of I_z^r is assumed negative over the given region. From the equation for v in eq. 15, this implies that v decreases with increasing time, and similarly for y_z in the reference solution. Thus, this choice of sign implies that the direction of the image strips is outwards at the limb, towards the invisible region.

An explicit solution for $v(t)$ is:

$$v(t) = v_0 \exp\left(-\int_{t_0}^{t} dt \left|\frac{I_z^r}{y_z}(1 + w^2 + v^2)^{1/2}\right|\right). \tag{17}$$

Clearly, because y_z goes to zero at the limb, v is forced towards 0 as an image strip approaches the limb. Similarly, w is forced towards y_x. If the image strip does intersect the limb, and if

along this curve $y_z/(t-t_{\rm int})$ is bounded, where $t_{\rm int}$ is the time of intersection, then w, v actually obtain their target values on the limb. It will be demonstrated later that this in fact occurs.

As an aside, note that the evolution equations can be written in the non–singular form,

$$\frac{d\vec{r}}{dt'} = y_z(\hat{L} - (\hat{n}\cdot\hat{L})\hat{n})$$

$$\dot{w} = (I^r_x y_z + I^r_z(w - y_x))(1 + w^2 + v^2)^{1/2}$$

$$\dot{v} = vI^r_z(1 + w^2 + v^2)^{1/2}, \tag{18}$$

by a redefinition of the time parameter. The limb now represents a line of attractive fixed points, with w and v taking their universal values there. This has been noticed previously by Saxberg [15], although his formulation of the equations is different.

The possibility of multiple solutions to shape from shading arises from the following fact: although v and $w - y_x$ must scale to zero with y_z near the limb, their absolute scale is not determined. Thus, we again define new variables

$$s \equiv \frac{v}{y_z}, \qquad r \equiv \frac{w - y_x}{y_z}. \tag{19}$$

The time evolution equation for s is:

$$\dot{s} = \frac{s}{y_z}(I^r_z D^{1/2} - \dot{y}_z), \tag{20}$$

where

$$D \equiv 1 + w^2 + v^2 = 1 + y_z^2 s^2 + (y_z r + y_x)^2. \tag{21}$$

Since

$$\left.\frac{\partial}{\partial x}\right|_y = \left.\frac{\partial}{\partial x}\right|_z - \frac{y_x}{y_z}\left.\frac{\partial}{\partial z}\right|_x, \qquad \left.\frac{\partial}{\partial y}\right|_x = \frac{1}{y_z}\left.\frac{\partial}{\partial z}\right|_x, \tag{22}$$

the time evolution of y_z is:

$$\dot{y}_z = \dot{x}(y_{zx} - \frac{y_x}{y_z}y_{zz}) + \dot{y}\frac{y_{zz}}{y_z}.$$

Substituting eq. 7 into this equation yields:

$$\dot{y}_z = \frac{1}{y_z}\left((y_{zx}y_z - y_x y_{zz})(L_x - I\frac{y_z r + y_x}{D^{1/2}}) + y_{zz}(L_y + \frac{I}{D^{1/2}})\right). \tag{23}$$

From the equation for I, eq. 1,

$$I_z^r = \frac{(y_{xz}, 0, y_{zz}) \cdot \hat{L}}{D_r^{1/2}} - \frac{I}{D_r}(y_x y_{xz} + y_z y_{zz}), \tag{24}$$

where

$$D_r \equiv 1 + y_x^2 + y_z^2. \tag{25}$$

Combining the above equations,

$$\dot{s} = \frac{s}{y_z^2}\left[\frac{y_z D^{1/2}}{D_r^{1/2}}(y_{xz}L_x + y_{zz}L_z) - \frac{y_z D^{1/2}}{D_r} I(y_x y_{xz} + y_z y_{zz})\right.$$

$$\left. -(y_{xx}y_z - y_x y_{zz})(L_x - I\frac{y_z r + y_x}{D^{1/2}}) - y_{zz}(L_y + \frac{I}{D^{1/2}})\right]. \tag{26}$$

The y_{zz} terms within the square brackets combine to give:

$$y_{zz}\left(L_z y_z \frac{D^{1/2}}{D_r^{1/2}} + y_x L_x - y_x(y_z r + y_x)\frac{I}{D^{1/2}} - (L_y + \frac{I}{D^{1/2}}) - I y_z^2 \frac{D^{1/2}}{D_r}\right) \equiv y_{zz} A. \tag{27}$$

Since

$$y_x L_x + y_z L_z = L_y + I D_r^{1/2}, \tag{28}$$

A can be rewritten:

$$L_z y_z(\frac{D^{1/2}}{D_r^{1/2}} - 1) + I(D_r^{1/2} - \frac{1 + y_x^2 + y_x y_z r}{D^{1/2}} - y_z^2 \frac{D^{1/2}}{D_r}). \tag{29}$$

Similarly, the y_{xz} terms in the square bracket combine to:

$$y_{xz} y_z \left(L_x(\frac{D^{1/2}}{D_r^{1/2}} - 1) - I y_x(\frac{D^{1/2}}{D_r} - \frac{1}{D^{1/2}}) + \frac{I y_z r}{D^{1/2}}\right) \equiv y_{xz} B. \tag{30}$$

It is easy to check from the expressions above that the terms in square brackets are of order y_z^2 as $y_z \to 0$ on the limb. *Thus the evolution equation for s is well defined at the image boundary.*

In fact, on the limb,

$$\frac{A}{y_z^2} = \frac{L_z y_x r}{1 + y_x^2} + \frac{I}{2(1 + y_x^2)^{1/2}}(s^2 + \frac{r^2}{1 + y_x^2} - 2), \tag{31}$$

and

$$\frac{B}{y_z^2} = \frac{L_x y_x r}{1+y_x^2} + \frac{Ir}{(1+y_x^2)^{1/2}} \frac{1-y_x^2}{1+y_x^2}. \tag{32}$$

The equation for r can be derived similarly:

$$\dot{r} = \frac{I_x^r D^{1/2} - \dot{y}_x}{y_z} + r\left(\frac{I_z^r D^{1/2} - \dot{y}_z}{y_z}\right). \tag{33}$$

The second term has already been examined above, and shown to have a well defined limit on the limb. In the first term, I_x^r is given by the expression for I_z^r above, eq. 24, with y_{xz}, y_{zz} replaced by y_{xx}, y_{xz}, respectively. Making the same replacements in eq. 23 for $\dot{y}_z$ yields an expression for $\dot{y}_x$. Thus

$$\dot{r} = \frac{1}{y_z^2}\left(A(y_{zz}r + y_{xz}) + B(y_{xz}r + y_{xx})\right). \tag{34}$$

As before, A/y_z^2 and B/y_z^2 are well defined on the occluding boundary as functions of y_z, y_x, r, and s.

y_z is not a continuously differentiable function of the image plane coordinates x and y. Thus we replace the variable y by $z_r(x,y)$, the value of z for the reference solution given x, y. The differential equation for the time evolution of z_r is:

$$\dot{z}_r = -\left(\frac{y_x}{y_z}\right)\left(L_x - \frac{I}{D^{1/2}}(ry_z + y_x)\right) + \frac{1}{y_z}\left(L_y + \frac{I}{D^{1/2}}\right)$$

$$= L_z + \frac{y_x Ir}{D^{1/2}} + \frac{I}{y_z D^{1/2}}(-D_r^{1/2} D^{1/2} + 1 + y_x^2). \tag{35}$$

Again, it is clear that this is well defined on the limb when $y_z = 0$. The system of equations for $\mathbf{P} \equiv (x, z_r, s, r)$ is consistent and *differentiable everywhere including on the limb.* Let the limb considered as a curve in the x–y plane be parameterized by σ. For arbitrary choice of initial conditions for s, r on the limb, the usual theorems of differential equations state that there exists a unique solution of the system of differential equations, with $\mathbf{P}$ a differentiable function of σ and t. Given this solution, y and z can also be computed by simple integration of their equations of motion.

It now remains to show that $w = y_x$, $v = y_z$, and that the parametric form expressing x, y, z in terms of t and σ can be converted into a surface function $y(x,z)$ or $z(x,y)$. Consider $U \equiv \dot{y} - w\dot{x} - v\dot{z}$. By direct computation, using the expressions above for the time derivatives, one can show that U vanishes everywhere. Next consider $V \equiv y_\sigma - wx_\sigma - vz_\sigma$. We want to demonstrate that this also vanishes. Define:

$$V_o \equiv \frac{V}{v} = qy_\sigma + px_\sigma - z_\sigma, \tag{36}$$

$$U_o \equiv \frac{U}{v} = q\dot{y} + p\dot{x} - \dot{z} = 0. \tag{37}$$

Away from the limb,

$$\frac{\partial V_o}{\partial t} - \frac{\partial U_o}{\partial \sigma} = \frac{\partial V_o}{\partial t} = p_\sigma \dot{x} - \dot{p}x_\sigma + q_\sigma \dot{y} - \dot{q}y_\sigma = \frac{\partial H}{\partial \sigma} = 0. \tag{38}$$

(Since $0 = H \equiv I + \hat{n} \cdot \hat{L}$ is true on the limb, and preserved by the differential equation, it is true for all t, σ.) Thus

$$V = vf(\sigma), \tag{39}$$

for some function $f(\sigma)$ which is independent of time. This is true on the limb as well by the smoothness of the solutions to the differential equations. We require $V = 0 = f(\sigma)$, which is equivalent to requiring $\dot{V} = 0$ everywhere on the limb. Explicitly, on the limb,

$$\frac{\partial V}{\partial t} = (\frac{\partial y_x}{\partial \sigma}, 0, \frac{\partial y_z}{\partial \sigma}(= 0)) \cdot \hat{L} - \frac{I}{(1+y_x^2)^{1/2}} y_x \frac{\partial y_x}{\partial \sigma}$$

$$-(I_x^r + I_z^r r)(1+y_x^2)^{1/2}\frac{\partial x}{\partial \sigma} - sI_z^r(1+y_x^2)^{1/2}\frac{\partial z}{\partial \sigma}. \tag{40}$$

Requiring this to vanish places one constraint on the choice of boundary conditions for the triple $(r(\sigma),\ s(\sigma),\ R)$, with

$$R \equiv \frac{\partial z}{\partial \sigma} / \frac{\partial x}{\partial \sigma}. \tag{41}$$

If the boundary conditions obey this constraint, $U = V = 0$ everywhere as desired.

As long as the Jacobian,

$$\begin{vmatrix} x_\sigma & z_\sigma \\ x_t & z_t \end{vmatrix}, \tag{42}$$

is non–vanishing, then one can replace the parametric variables σ and t by the coordinates x and z. A non–vanishing Jacobian can be obtained by simply choosing the function $z(\sigma)$ to avoid this case. Also, since this can be assumed to hold for the reference solution, it will hold also for perturbations of this solution. A differentiable surface function $y(x,z)$ is thereby obtained. Moreover, by the above result for the vanishing of U, V, and the non–vanishing of the Jacobian, one has

$$w = \frac{\partial y}{\partial x}, \qquad v = \frac{\partial y}{\partial z}, \tag{43}$$

where this refers to the actual solution y rather than the reference solution.

Similarly, as long as

$$\begin{vmatrix} x_\sigma & z^r_\sigma \\ x_t & z^r_t \end{vmatrix} \neq 0, \tag{44}$$

the solution may be parameterized locally by z^r and x. This implies that $z(x,\ y)$ is a well defined function, i.e. that the surface is not self–occluding. Thus it has been established that there is a range of possible solutions specified by 1) the choice of $z(x,y)$ on the limb, and 2) by the choice of a combination of the parameters $s(x,y)$ and $r(x,y)$ on this boundary. There is thus a *two parameter ambiguity* for the shape solution in the neighborhood of the limb, as opposed to the one parameter ambiguity around an interior image curve [3].

The evolution equations for $\mathbf{P}$ are non–singular on the limb, and in fact there is no problem in extending them past the limb, as long as the parameters of the reference solution are known in this unseen region. For a characteristic strip that intersects the limb, s and r will be finite at the point of intersection since the right hand sides of their evolution equations are bounded. Since however $y_z = 0$ there, $w = y_x$ and $v = y_z = 0$ are forced on the limb, as stated earlier.

Lastly, because of its relevance to the next section, we consider the case where the surface is specified on an interior image curve with one endpoint on the limb. The depth variation on the curve can be specified arbitrarily, as long as it is smooth (as a function of x and z^r) and consistent with the image intensities. The choice of depth also determines the parameters s and r on the curve as the solutions of quadratic equations, and therefore up to a two–fold ambiguity in general. Again, because the equations for $\mathbf{P}$ are blind to the occluding boundary, there is no problem in extending this space curve to a surface solution parameterized by the time t and the σ parameter for the initial curve. As long as the characteristic strips in the z–x plane are

transverse to the initial line, then one can show as above that a local surface solution exists around the initial line. This step is easier, in fact, since the requirement that V vanishes on the initial line implies directly that $f(\sigma) = 0$. As before, this result extends to the limb by smoothness.

6. Shape from Shading as a Partially Ill–Posed Problem

It is demonstrated numerically in this section that image regions where shape from shading is ill–posed appear in images of very simple objects, and that this occurs even though the image contains the occluding boundary and singular points. Our example is essentially an elongated egg–shape, viewed from a direction reasonably distinct from the long axis of the egg. This numerical result agrees with intuition based on the results of the last section.

The surface we consider is, in a body–centered coordinate system:

$$x_b^2 + y_b^2 + \frac{|z_b|^3}{27} = 1. \tag{45}$$

In this coordinate system, the light source direction is:

$$\hat{L}_b = (1, -1, 5), \tag{46}$$

and the viewing direction is:

$$\vec{v}_b = (-\sin, 0, \cos), \qquad \sin = .15, \quad \cos = (1 - \sin^2)^{1/2}. \tag{47}$$

The object is considered to be at positive z with respect to the viewer. The flow of the characteristic strips projected into the image plane is shown in Figure 1. The lines without arrows represent the flow in the region of the object that is visible but not illuminated. Here and below, the x direction is represented along the vertical axis, and the y or z direction on the horizontal axis—the opposite of the usual convention.

The occluding boundary is characterized by

$$\vec{v} \cdot \hat{n} = 0, \tag{48}$$

where $\hat{n}$ is the surface normal. Explicitly,

$$y_{bx}|_{z_b} = -\left(\frac{x_b}{y_b}\right),$$

$$y_{bz}|_{x_b} = -1.5\left(\frac{z_b|z_b|}{27y_b}\right), \tag{49}$$

$$\hat{n} \sim (-y_{bx}, 1, -y_{bz}) \sim \left(x_b, y_b, 1.5\frac{z_b|z_b|}{27}\right). \tag{50}$$

The equation for the occluding boundary is

$$-x_b \sin + 1.5\frac{z_b|z_b|}{27}\cos = 0. \tag{51}$$

Since we will be interested only in the region of the object near $y_b = 1$, y_b will be assumed positive from now on. In Figure 2 the positive y_b half of the object described by eq. 45 is displayed. The object is shown in a rotated coordinate system so that the occluding boundary with respect to the viewer direction is visible. It is represented by a solid line. In this Figure, the horizontal axis represents a vector fairly close to the z_b direction, so that more of the length of the object along the z_b direction is displayed.

We shall work below in the viewer coordinate system which is related to the body-centered system above by:

$$\begin{pmatrix} x \\ y \\ z \end{pmatrix}_v = \begin{pmatrix} \cos & 0 & \sin \\ 0 & 1 & 0 \\ -\sin & 0 & \cos \end{pmatrix} \begin{pmatrix} x \\ y \\ z \end{pmatrix}_b. \tag{52}$$

Below, the subscript v identifying the viewer system will be omitted. Clearly, in this system

$$\vec{v} = (0, 0, 1). \tag{53}$$

In Figure 3, a portion of the surface and occluding boundary is displayed projected into the z–x plane in the new coordinate system. The flow of characteristics is also shown. Again, the x axis is vertical. The important point, which is clear from Figure 3 and also can be seen in Figure 2, is that there is a region that is bounded above by a characteristic strip line, and below by the limb. The bounding characteristic strip is represented as a solid line, and is obtained by numerical integration. The corresponding image region is *isolated*: points in this region are unconnected to the rest of the image by any characteristic strip in the image. (Of course, they are connected to the rest of the image by characteristic strips passing through the invisible part of the object beyond the limb.) According to our previous results, the shape solution is only

constrained for points that can be connected by visible characteristic strips to singular points in the image. Thus one might expect that there would be many shape solutions for the given image region—that shape from shading would be ill–posed there—even with the shape solution for the rest of the image fixed to be as in eq. 45. This is what will be demonstrated numerically. From now on we focus exclusively on the region defined above, referred to as the *ill–posed region* of the image.

The ill–posed region projected in the image plane is shown in Figure 4. The scale of the horizontal axis is greatly expanded—y ranges only between .976 and 1, and it is clear that the ill–posed region is only a very insignificant fraction of the whole image. The range in x is .385. The lower, short, horizontal line indicates the lower limit of the ill–posed region. At this point, the bounding characteristic strip becomes tangent to the occluding boundary. The upper, short horizontal solid line indicates a second point on the occluding boundary where a (different) characteristic strip is tangent to the boundary. This tangency is apparent in Figure 3.

Our strategy for generating new solutions corresponding to the ill–posed image region is as follows. We take as our initial image curve the line of constant x corresponding to the upper horizontal solid line in Figure 4. For the exact solution, it is clearly transverse to every characteristic strip. Next, the depths for this initial curve are perturbed from their original values of eq. 45. If the perturbation is moderate, the characteristic curves projected into the x–z plane will continue to be transverse to the initial line for the perturbed case, and the Jacobian in eq. 42 will be non–vanishing. This must be true at the point where the initial line intersects the limb, since the tangent to the characteristic strip is determined there. Rather than posing a difficulty, as it would for the original singular form of the evolution equations in 7 and 10, this point is actually better constrained than points in the interior of the image.

The results of the previous section then imply that there exists a locally valid solution containing the perturbed space curve. Moreover, we expect no difficulty in extending the local solution via the characteristic strips to the limb. For a moderate perturbation, all characteristic strips should continue to reach the limb. The limb will continue to represent the occluding boundary for the perturbed solution. Lastly, the limb introduces no particular tendency for the characteristic strips to cross in the x–z plane, implying that a consistent surface solution $y(x, z)$ exists. Below, experimental results supporting these assertions are presented.

We reemphasize that what has been proven analytically is the existence of a local solution around the initial line described above. It is not known a priori how far this locally valid solution can be extended in the image, however, it has been demonstrated that there is no difficulty in prinicple in extending the solution to the limb. Whether this is possible in any particular case must be settled by experiment. Our numerical experiments show that for the perturbed solutions that we have examined, the characteristic strips are extremely well behaved, and there is no hint of trajectory crossing in the z–x or z_r–x planes. There appears to be no difficulty in deriving multiple shape solutions corresponding to the ill–posed region in the image.

For our experimental results, $z(y)$ is perturbed on the initial line described above by:

$$z(y) = z_s + f(y - y_c)^2. \tag{54}$$

z_s represents the standard value of z obtained by solving eq. 45 for the given values of x and y, f is an arbitrary constant giving the scale of the perturbation, and y_c indicates the y coordinate of the point where the initial line intersects the bounding characteristic strip. Explicitly, $y_c = .998574791829$. The initial line is characterized by $x = x_{\tan} = .070495571762$. It intersects the limb at $y = .999177802152$. Thus the range of y over the initial line is only .0006.

The perturbation is chosen quadratic so that both it and its derivative with respect to y vanish at $y = y_c$, on the bounding characteristic strip. This ensures that the solution in the ill–posed region will join smoothly onto the fixed solution in the rest of the image. The solution on the bounding characteristic strip is the same for the perturbed and unpertubed solutions. Also, at the limb, the perturbation has finite derivative with respect to y. Therefore, $y_z = 0$ and y_x is the same as for the standard solution, as is required since this quantity is fixed by the limb.

We have computed the characteristic strips using the evolution equations both in their singular version of eq. 15, and in the non–singular version of eqs. 20 and 33, obtaining consistent results. To integrate these equations, starting values for $w = y_x$ and $v = y_z$, or equivalently r, s, are required on the initial line. y_z can be directly determined from the known function $z(y)$ on the initial line. y_x is determined from eq. 1 as the root of a quadratic equation. The two–fold ambiguity is resolved by choosing the same root as for the standard solution.

Solutions are generated by integrating the characteristic strips transverse to the initial line in the z–x plane. The values of x, y, z can be explicitly determined all along the integrated strips. The existence of a valid perturbed solution is dependent on the non–crossing of the characteristic trajectories in the z–x and z_r–x planes, and on the Jacobian non–vanishing condition remaining valid. All these conditions will be seen to hold true.

We first integrated the exact solution, taking $f = 0$. Since the surface is known, the characteristic strips can be obtained either by integrating the complete system of equations, or else just eq. 7. The results obtained are the same, and are shown in Figure 5. The characteristic strips in the z–x plane are almost parallel straight lines. The leftmost of these is the bounding characteristic strip. The initial line is given by the short horizontal line. The accuracy of the integration is better than 10^{-12}.

In Figure 6, we display our results for a perturbation scaled by $f = 10^6$. With f of this magnitude, the perturbation is comparable in size to the amount by which z varies over the initial line in the standard solution. The display scale has been enlarged by about twenty percent along the horizontal z axis, while the vertical scale is the same as in the previous Figure. Again, the leftmost line is the bounding characteristic strip, and the horizontal line is the intial line. The occluding boundary is not displayed explicitly since it is not known analytically for this case, but it is given by the smooth curve passing through the ends of the displayed strips. In Figure 7, the characteristic strips are displayed in terms of the coordinates x and z_r. The fact that they do not intersect shows that the recovered surface is not self–occluding from the viewer's perspective. Also, the length of the characteristic strips is approximately proportional to the evolution time, so the initial line under time evolution remains transverse to the characteristic strips, and the Jacobians of eqs. 42 and 44 remain non–zero as required. Finally, in Figures 8–11 the recovered surface is shown from various angles. The perturbed surface recovered for the ill–posed region is shown by itself, and together with the known solution of eq. 45. The perturbed surface joins smoothly onto the standard solution along one side, as it must since they both share the bounding characteristic. However, the difference in the two surfaces is clear at the limb, where there is a sharp discontinuity from the perturbed to the standard surface. The scale of the display has been exagerated for better visibility.

In Figures 12–17 are shown the equivalent results for a perturbation scaled by $f = 2(10^6)$.

Clearly, this yields yet another surface solution in the ill–posed region. These new solutions were derived for *arbitrary* perturbation of the depths on the initial image line described above. Thus, it is almost certain that similar results would have been obtained for many different choices of initial conditions. This implies the likelihood that there are infinitely many solutions corresponding to the ill–posed region, and that shape from shading is in fact ill–posed in this region.

In order to demonstrate that ill–posed regions need not always be tiny, we present a second image example. However, it is somewhat contrived, since the sole singular point in the image is very close to the limb, and such an image would be very difficult to reconstruct anyway because of the large gradients.

In a body–centered coordinate system, the object is given by:

$$A + B^2 + \frac{z^2}{64} = 1,$$

where

$$A = \left\{ \begin{array}{ll} .8x + .56 & x \geq -.5 \\ (x + .9)^2 & x < -.5 \end{array} \right\},$$

$$B = \left\{ \begin{array}{ll} y & x \geq 0 \\ y + x^2 & x < 0 \end{array} \right\}. \tag{55}$$

The illumination is from above, with $\hat{L} = -\hat{z}$. The characteristic strips are therefore the lines of steepest descent, or fall lines, in z. The viewing direction is

$$(0, \cos\theta, -\sin\theta), \tag{56}$$

with $\sin\theta = .15$. There is a unique singular point in the image, which is a source.

The illuminated portion of the object is displayed projected into the x–y plane in Figure 18, together with the flow field for the characteristic strips. In this Figure, the standard convention (x axis horizontal, y axis vertical) is used, unlike the previous figures. The visible points are identified by complete arrows, while those points that are occluded in the image have partial arrows. The occluding boundary can be located roughly as a line dividing the regions of complete and incomplete arrows. The characteristic strips are the integral curves of this flow.

Consider the characteristic strips in the upper right portion of Figure 18. It should be fairly clear that they cross the occluding boundary at the left heading rightwards into the visible region, and exit the image at the right boundary (the shadow boundary). Thus the whole upper visible region in Figure 18 is unconnected to any singular point in the image, and is an ill–posed region of the type discussed above.

The flow of characteristic strips in the image plane is displayed in Figure 19. The sole source is located at the top of the Figure. Again, the behavior of the characteristic strip lines should be readily apparent. The horizontal x–axis is the same in both Figures, so that the strips in the Figures can be identified according to the x–coordinate at which they exit the image. It is clear that the ill–posed region in the image is not as dramatic as it seemed in Figure 18. It is probably on the order of of a fifth of the whole image, bounded on the left by an image strip, and on the right by the image boundary.

We have not actually verified that there are multiple solutions to shape from shading for the identified ill–posed region in this example. The example is intended to demonstrate only that such regions can be respectable fractions of the whole image. When the image described above is displayed, it does seem difficult to interpret towards the right of the image, probably appearing shallower than in reality. However, the interpretation of simulated images is not reliable in general, because of the unnatural assumptions of a single point light source (the shadow boundary always looks like an occluding boundary), and no specularity.

7. Image Regions Bounded by the Arms of a Saddle

In this section is presented another example of a region–type where the shape may be ill–posed or difficult to reconstruct. The examples of this and the previous section certainly do not exhaust the possibilities for ill–posed regions, although perhaps they are among the more frequently–occurring. Other possibilites will be considered in future work. In the current example, we describe a region that is isolated from any elliptical–type singular point by being trapped between a saddle point and the limb. Recall that at a saddle point there are only four image strips that actually connect to the point—most image strips bypass the saddle point, although they may approach it closely. In the example, all four of these special image strips connect the saddle point to the limb rather than to a visible singular point, and thus divide the

image into four sectors. Two of these contain no singular point, so that the shape solution in these sectors is constrained only by the saddle point, if at all—they are isolated from the rest of the image by the image strips connecting to the saddle point. Although it has been shown that for illumination symmetric around the viewer direction saddle points do constrain the shape solution [9], it remains unsettled whether this is still true for general illumination. If not, then the shape reconstruction problem in the two sectors above may be ill–posed. Even if the result generalizes, since it is valid locally only, the shape in some part of these sectors may be ill–posed.

In the most optimistic case, it still may be difficult to reconstruct the shape algorithmically in these sectors. For elliptical–type singular points, the shape solution is the (un)stable manifold, and, as its name implies, can be determined with relative stability via the Lambda Lemma [15]. There is no such stability for the solution around a saddle singular point. From a different viewpoint, the image strips around an elliptical singular point connect to the point, with initial condition fixed by the point, and they can easily be integrated outwards to generate a solution. In contrast, it is not clear how to fix the initial conditions for the image strips in the neighborhood of a saddle singular point. Most of these strips do not approach the point closely. This remains a topic for future study.

The example surface is described by:

$$(x^2 - .81)^2 + (y + x^2)^2 + z^2/64 = 1.$$

A top view of the object projected into the x–y plane is shown in Figure 20, with the characteristic flow displayed. The object is illuminated from above, i.e. $\hat{L} = -\hat{z}$. The characteristic flow vectors therefore represent the downwards direction. In this Figure, the standard convention (x axis horizontal, y axis vertical) is used, as for the second example in the previous section. The object is symmetric around the y axis. It can be characterized as a ridge extending like two arms towards the negative y direction. The saddle point is the low point on the ridge and is situated at $x = 0$, in the center of the Figure, just below the solid line.

The viewing direction is close to the y direction:

$$\hat{v} = (0,\ \cos,\ -\sin), \tag{57}$$

with sin = .01. The solid line represents the occluding boundary for this viewing direction.

Two image strips connecting to the saddle point lie on the y axis, diverging from the given point. It is clear by inspection that there are approximately horizontal image strips connecting the saddle point to the occluding boundary. The region embraced by these horizontal strips and the occluding boundary is isolated from the two source points which are the maxima of z on the object. Thus, the region is potentially ill–posed, as described above. Note that it is small, however.

8. Appendix: Proof of the Theorem on Generic Surfaces

Definition: A smooth, real–valued function on a manifold M is a *Morse function* if its critical points are all non–degenerate.

Lemma 1: *Every smooth, closed, orientable surface S embedded in R^3 can be approximated arbitrarily well by one whose height function is a Morse function.* [8] [4].

Proof: Let h denote the height function on the surface S. We use the following result. **Theorem**: *every smooth, real–valued function on a compact manifold M can be uniformly approximated by a Morse function on M* (see, e.g., [8] [4]). Let $g = h + \delta h$ be such a Morse function approximation to h. We may take

$$\delta h = \vec{a} \cdot (x, y, z), \tag{58}$$

for some vector $\vec{a}$ of arbitrarily small magnitude [4]. Define a C^∞ function $\epsilon(x)$ satisfying $|\epsilon(x)| \leq 1$, and

$$\epsilon(x) = \left\{ \begin{array}{ll} 0 & |x| \leq \cos(\theta_2) \\ 1 & |x| \geq \cos(\theta_1) \end{array} \right\},$$

where $0 < \theta_1 < \theta_2 < \pi/2$. Denote by $\cos(\theta)$ the real–valued function on the surface S which gives the cosine of the angle between the height direction $\hat{z}$ and the surface normal $\hat{n}$ for each point on S. Thus, $\cos(\theta) = \hat{n} \cdot \hat{z}$. Finally, define the function

$$g' = h + \epsilon(\hat{n} \cdot \hat{z}) \delta h. \tag{59}$$

We claim that g' is a Morse function on S if $|\vec{a}|$ is chosen sufficiently small. This is fairly clear since $g' = g$ in the region where there are critical points, and $g = h$ only in the region with $\hat{n} \cdot \hat{z} \leq \cos(\theta_2)$, where h has no critical points.

What we need to show is that g' also has no critical points in the region R, where $|\hat{n} \cdot \hat{z}| \leq \cos(\theta_1)$. At any point p in this region, one can erect a local coordinate system $(\xi_1,\ \xi_2)$, given by the projection of the surface onto the directions

$$\hat{\xi_1} \equiv \frac{\hat{n}\ \mathrm{x}\ (\hat{z}\ \mathrm{x}\ \hat{n})}{|\hat{n}\ \mathrm{x}\ (\hat{z}\ \mathrm{x}\ \hat{n})|},$$

$$\hat{\xi_2} \equiv \frac{\hat{z}\ \mathrm{x}\ \hat{n}}{|\hat{z}\ \mathrm{x}\ \hat{n}|}. \tag{60}$$

$\hat{\xi_1}$ lies in the direction of steepest ascent. To demonstrate that p is not a critical point of g', consider the derivative:

$$\left.\frac{\partial g'}{\partial \xi_1}\right|_{\xi_2} = \frac{\partial h}{\partial \xi_1} + \vec{a} \cdot \frac{\partial \vec{r}}{\partial \xi_1}\epsilon + \vec{a} \cdot \vec{r}\frac{\partial \epsilon}{\partial \xi_1}, \tag{61}$$

where

$$\vec{r} \equiv (x,\ y,\ z). \tag{62}$$

We have:

$$\left.\frac{\partial \vec{r}}{\partial \xi_1}\right|_{\xi_2} = \hat{\xi_1}, \tag{63}$$

and therefore:

$$\left.\frac{\partial h}{\partial \xi_1}\right|_{\xi_2} = \hat{\xi}_{1z} = |\sin(\theta)| \geq \sin(\theta_1),$$

since $h = z$. One can find a bound B, such that

$$\left|\frac{\partial \epsilon}{\partial \xi_1}\right| < B, \tag{64}$$

and a bound B' such that $|\vec{r}| < B'$, for every point in the region R, since it is compact. Then if

$$|\vec{a}| < \frac{\sin(\theta_1)}{4BB'},$$

it is clear that

$$\left.\frac{\partial g'}{\partial \xi_1}\right|_{\xi_2} \neq 0, \tag{65}$$

at every point in R, so that it contains no critical points. Therefore g' is a Morse function on S.

Lastly, we find a surface which has g' as its height function. The existence of such a surface proves the lemma. Consider the regions of the surface where

$$|\cos(\theta)| > \cos(\theta_3), \tag{66}$$

where $0 < \cos(\theta_3) < \cos(\theta_2)$. For points in these regions, one can erect local coordinate systems parameterizing the surface by its projection in the x–y plane. Define the perturbed surface to be given by the graph of g' over the region above, and equal to the original surface over the complement of this region. The join of these two surfaces is smooth, since $g' = h$ in a neighborhood of the boundary between them. Q.E.D.

Also, note that if the original surface S in the above lemma is non–self–intersecting, then one can choose the surface perturbation small enough so that the approximating surface is also non–self–intersecting.

Lemma 2: *Let S be a smooth, closed surface in R^3, whose height function is a Morse function. Then S can be approximated arbitrarily well by a surface whose height function is a Morse function, and on which there are no saddle connections.*

Proof: Suppose that S has a saddle connection line l. By definition, l is the intersection of the stable manifold of one saddle point with the unstable manifold of another, for the dynamical system:

$$\frac{d\vec{r}}{dt} = \hat{z} - (\hat{n} \cdot \hat{z})\hat{n}. \tag{67}$$

We will demonstrate that a small perturbation in the surface can shift the unstable manifold line slightly, so that it no longer intersects the stable manifold line from the upper saddle point.

Choose a point p on l such that the surface normal $\hat{n}$ at p obeys $1 > |n_z| > 0$. Such a point p must exist since the saddle points are non–degenerate. In some neighborhood of p, the surface can be parameterized by coordinates ξ_1, ξ_2 such that 1) the flow lines in these coordinates are straight lines in the the ξ_1 direction, and 2) $\partial z/\partial \xi_1 = 1$ along these lines, so that the lines of constant ξ_1 are also lines of constant z, 3) p is the origin. This follows from the Tubular Flow Theorem [11]. The ξ coordinates are closely related to those in the previous Lemma. l over this neighborhood is given by $\xi_2 = 0$.

Define a rectangular region R in the ξ coordinates small enough so that the corresponding surface region can also be parameterized by x and y. Then, the ξ coordinates can be thought of as parameterizing a region of the x–y plane. Label this region of the x–y plane by R also. We will now define a smaller region $R' \subset R$ in the x–y plane, on which the surface will be perturbed. In the ξ coordinate system: 1) R' is rectangular, 2) R and R' are positioned symmetrically about the origin p, 3) $(L_1,\ L_2)$ and $(L_1',\ L_2')$ respectively represent the dimensions of R and R'.

Within R', $z(\xi_1, \xi_2)$ will be perturbed by $\delta z(\xi_1, \xi_2) = \psi(\xi_1)\phi(\xi_2)$. ψ and ϕ are non–negative C^∞ functions with the following properties.

$$\left\{ \begin{array}{ll} \phi(\xi_2) = 0, & |\xi_2| \geq \frac{L_2'}{4} \\ \frac{\partial \phi}{\partial \xi_2} > 0, & |\xi_2| \leq \frac{L_2'}{8} \end{array} \right\},$$

$$\left\{ \begin{array}{ll} \psi(\xi_1) = 0, & |\xi_1| \geq \frac{L_1'}{4} \\ \psi(\xi_1) \neq 0, & |\xi_1| < \frac{L_1'}{4} \end{array} \right\}, \tag{68}$$

Also, we assume $|\partial\psi/\partial\xi_1|$ is bounded by H, and $|\partial\phi/\partial\xi_2|$ by F.

The surface strip entering the region R' at $(-L_1'/2,\ 0)$ originates at a saddle point, by assumption, and is part of the unstable manifold of this point. On the perturbed surface, we will refer to this line and its continuation as l'. We are interested in finding the ξ_2 value at which l' exits the region R. First, an equation for the flow in the ξ coordinates is derived.

$$\frac{d}{dt}\begin{pmatrix} \xi_1 \\ \xi_2 \end{pmatrix} = \left[\frac{\partial(\xi_1, \xi_2)}{\partial(x, y)}\right]\begin{pmatrix} \dot{x} \\ \dot{y} \end{pmatrix}, \tag{69}$$

where:

$$\left[\frac{\partial(\xi_1, \xi_2)}{\partial(x, y)}\right] \equiv \begin{pmatrix} \frac{\partial \xi_1}{\partial x} & \frac{\partial \xi_1}{\partial y} \\ \frac{\partial \xi_2}{\partial x} & \frac{\partial \xi_2}{\partial y} \end{pmatrix}. \tag{70}$$

On the perturbed surface, from eq. 67,

$$\begin{pmatrix} \dot{x} \\ \dot{y} \end{pmatrix} = N\begin{pmatrix} \frac{\partial(z+\delta z)}{\partial x} \\ \frac{\partial(z+\delta z)}{\partial y} \end{pmatrix}, \tag{71}$$

with N a normalizing factor,

$$N \equiv \left[1 + \left(\frac{\partial(z+\delta z)}{\partial x}\right)^2 \left(\frac{\partial(z+\delta z)}{\partial y}\right)^2\right]^{-1}. \tag{72}$$

Finally, one obtains:

$$\frac{d}{dt}\begin{pmatrix} \xi_1 \\ \xi_2 \end{pmatrix} = N\left[\frac{\partial(\xi_1,\xi_2)}{\partial(x,y)}\right]\left[\frac{\partial(\xi_1,\xi_2)}{\partial(x,y)}\right]^{\mathrm{T}}\begin{pmatrix} \frac{\partial(z+\delta z)}{\partial \xi_1} \\ \frac{\partial(z+\delta z)}{\partial \xi_2} \end{pmatrix}. \tag{73}$$

To evaluate the matrix appearing in this equation, we use the fact that:

$$\left[\frac{\partial(\xi_1,\xi_2)}{\partial(x,y)}\right] = \begin{pmatrix} \frac{\partial x}{\partial \xi_1} & \frac{\partial y}{\partial \xi_1} \\ \frac{\partial x}{\partial \xi_2} & \frac{\partial y}{\partial \xi_2} \end{pmatrix}^{-1}. \tag{74}$$

The $\hat{\xi}_1$ direction in the x–y plane is given by $\vec{\nabla} z$, since by assumption this coordinate parameterizes lines following the gradient of z. The $\hat{\xi}_2$ direction is perpendicular to this, since ξ_2 parameterizes lines of constant z. Therefore, $\hat{\xi}_1$ and $\hat{\xi}_2$ are given by eq. 60, and the two rows of $\partial(\xi_1,\xi_2)/\partial(x,y)$ are orthogonal. This implies:

$$\frac{d}{dt}\begin{pmatrix} \xi_1 \\ \xi_2 \end{pmatrix} = N\begin{pmatrix} \left(\frac{\partial \xi_1}{\partial x}\right)^2 + \left(\frac{\partial \xi_1}{\partial y}\right)^2 & 0 \\ 0 & \left(\frac{\partial \xi_2}{\partial x}\right)^2 + \left(\frac{\partial \xi_2}{\partial y}\right)^2 \end{pmatrix}\begin{pmatrix} \frac{\partial(z+\delta z)}{\partial \xi_1} \\ \frac{\partial(z+\delta z)}{\partial \xi_2} \end{pmatrix}, \tag{75}$$

The second property of the ξ coordinate system determines

$$\begin{pmatrix} \frac{\partial x}{\partial \xi_1} \\ \frac{\partial y}{\partial \xi_1} \end{pmatrix} = \frac{1}{(z_x^2 + z_y^2)^{0.5}}\begin{pmatrix} z_x \\ z_y \end{pmatrix}, \tag{76}$$

from which follows:

$$\begin{pmatrix} \frac{\partial \xi_1}{\partial x} \\ \frac{\partial \xi_1}{\partial y} \end{pmatrix} = \begin{pmatrix} z_x \\ z_y \end{pmatrix}, \tag{77}$$

Also, one can require that at p

$$(\frac{\partial \xi_2}{\partial x})^2 + (\frac{\partial \xi_2}{\partial y})^2 = 1. \tag{78}$$

Within R' the equations for the surface strips are:

$$\frac{d\xi_1}{dt} = \frac{z_x^2 + z_y^2}{1 + z_x^2 + z_y^2}\left(1 + \phi(\xi_2)\frac{\partial\psi}{\partial\xi_1}\right),$$

$$\frac{d\xi_2}{dt} = N\left[\left(\frac{\partial\xi_2}{\partial x}\right)^2 + \left(\frac{\partial\xi_2}{\partial y}\right)^2\right]\psi(\xi_1)\frac{\partial\phi}{\partial\xi_2}. \tag{79}$$

One can assume that the neighborhood R is small enough so that, throughout R,

$$\left|\left(\frac{\partial\xi_2}{\partial x}\right)^2 + \left(\frac{\partial\xi_2}{\partial y}\right)^2 - 1\right| < \epsilon, \tag{80}$$

for some small ϵ, and that

$$\frac{z_x^2 + z_y^2}{1 + z_x^2 + z_y^2} > A, \tag{81}$$

for some A. Also, we assume the surface perturbation is small, and, specifically, that

$$(FH)L_2' < \delta,$$

for some other small quantity δ . The time during which l remains in R' is less than

$$t_{\max} = \frac{L_1'}{A(1-\delta)}. \tag{82}$$

Lastly, we also require that

$$(FH)\frac{(L_1')^2(1+\epsilon)}{A(1-\delta)} < \frac{L_2'}{8}. \tag{83}$$

Then the trajectory l' always satisfies

$$\xi_2 < \frac{L_2'}{8}, \tag{84}$$

while it passes through R. Since $\frac{\partial\xi_2}{\partial t}$ is non-negative in this region, l' is displaced exclusively towards the positive ξ_2 direction. Thus, l' exits R at $(L_1/2,\ \bar{\xi}_2)$ with $\bar{\xi}_2 > 0$.

On the other hand, the trajectory originating as the stable manifold of the upper saddle point passes through the point $(L_1/2,\ 0)$. The later history of l' extends to higher z, and

therefore cannot include this point. Thus, the stable and unstable manifolds of the two saddles points no longer intersect. It is also clear that, for a small enough surface perturbation, no critical point has been introduced. Repeating this argument for every saddle connection of the original surface, one finally obtains a surface with no saddle connections. Q.E.D.

Lastly, to finish the proof of the Theorem of section 3, we must show that a perturbed structurally stable surface remains structurally stable, if the perturbation is sufficiently small. Consider therefore a structurally stable surface S, and let S' be a small perturbation of this surface. This means that S and S' are diffeomorphic, with a diffeomorphism close to the identity. Consider the vector field V_S given by $\hat{z} - (\hat{n} \cdot \hat{z})\hat{n}$ evaluated on S, and also the vector field $V_{S'}$ given by evaluating this expression on S'. Let $\bar{V}_{S'}$ be the pull-back of $V_{S'}$ onto the surface S. $\bar{V}_{S'}$ constitutes a perturbation of the vector field V_S on S. By assumption, V_S is a structurally stable vector field on S. But the theorems of Peixoto, and of Palis and Smale [11] [12], state that a sufficiently small perturbation of a structurally stable vector field is also structurally stable. Thus, $\bar{V}_{S'}$ can be assumed structurally stable. But this implies that S' is structurally stable. This proves the Theorem.

Acknowledgments

I would like to acknowlege useful and enjoyable conversations with B. Saxberg, Don O'Shea, B. K. P. Horn, and Richard Weiss.

References

1. A. R. Bruss, "The Eikonal Equation: Some Results Applicable to Computer Vision," *Journal of Math. Phys.* 23(5): 890-896, May 1982.

2. P. Deift and J. Sylvester, "Some Remarks on the Shape–from–Shading Problem in Computer Vision," *Journal of Mathematical Analysis and Applications*, Vol. 84, No. 1, pp. 235–248, November 1981.

3. P. R. Garabedian, *Partial Differential Equations.* John Wiley: New York, N. Y., 1969.

4. V. Guillemin and A. Pollack, *Differential Topology.* Prentice–Hall: New Jersey, 1974.

5. B.K.P. Horn, *personal communication.*

6. B.K.P. Horn and M.J. Brooks (eds.) *Shape from Shading.* MIT Press: Cambridge, MA, 1989.

7. B.K.P. Horn, "Height and Gradient From Shading," Massachusetts Institute of Technology AI Lab, Massachusetts Inst. Technol., Cambridge, MA, A.I. Memo. 1105, May 1989.

8. J. Milnor, *Morse Theory*, Annals of Mathematics Studies 51. Princeton University: New Jersey, 1970.

9. J. Oliensis, "Existence and Uniqueness in Shape From Shading," University of Massachusetts TR 89–109, October 1989.

10. J. Oliensis, "Existence and Uniqueness in Shape From Shading," to appear in the *Tenth International Conference on Pattern Recognition*, Atlantic City, New Jersey, June 17–21, 1990.

11. J. Palis and W. de Melo, *Geometric Theory of Dynamical Systems.* Springer-Verlag: NY, 1982.

12. J. Palis and S. Smale, "Structural Stability Theorems," in Proc. of Symposia in Pure Mathematics, Vol. 15, Berkeley, CA, July 1968, pp. 223-231.

13. B. Saxberg, *personal communication.*

14. B. Saxberg, "An Application of Dynamical Systems Theory to Shape From Shading," in Proc. DARPA Image Understanding Workshop, Palo Alto, CA, May 1989, pp. 1089-1104.

15. B. V. H. Saxberg, "A Modern Differential Geometric Approach to Shape from Shading," MIT Artificial Intelligence Laboratory, TR 1117, 1989.

16. P. Giblin and R. Weiss, "Reconstruction of Surfaces from Profiles," in Proc. International Conference on Computer Vision, London, England, June 1987, pp. 136-144.

Figure Captions

Figure 1. The characteristic flow on an object for which shape from shading is partially ill–posed.
Figure 2. A rotated view of the object in Figure 1.
Figure 3. The ill–posed region of the object of Figure 1, projected into the z–x plane.
Figure 4. The ill–posed region of the object of Figure 1, projected into the y–x plane.
Figure 5. The characteristic strip lines for the object of Figure 1, projected into the z–x plane.
Figure 6. The characteristic strip lines for the object of Figure 1, perturbed with $f = 10^6$, projected into the z–x plane.
Figure 7. The characteristic strip lines for the object of Figure 1, perturbed with $f = 10^6$, projected into the z_r–x plane.
Figure 8. A rear view of the surface recovered for $f = 10^6$, corresponding to the ill–posed region of the object in Figure 1. The position of the viewer is into the page.
Figure 9. The same view as in Figure 8 of the perturbed surface, shown together with the unperturbed surface. Note the sharp discontinuity at the occluding boundary.
Figure 10. A front view of the surface recovered for $f = 10^6$, corresponding to the ill–posed region of the object in Figure 1. The position of the viewer is out of the paper.
Figure 11. The same view as in Figure 10 of the perturbed surface, shown together with the unperturbed surface. Note the smooth joining of the two surfaces at a line corresponding to the bounding characteristic strip of the ill–posed region. The slight roughness of the join is due to the fact that the perturbed surface has been averaged over nearest neighbors so as to fill in holes.
Figure 12. The characteristic strip lines for the object of Figure 1, perturbed with $f = 2(10^6)$, projected into the z–x plane.
Figure 13. The characteristic strip lines for the object of Figure 1, perturbed with $f = 2(10^6)$, projected into the z_r–x plane.
Figure 14. A front view of the surface recovered for $f = 2(10^6)$, corresponding to the ill–posed region of the object in Figure 1. The position of the viewer is out of the paper.
Figure 15. The same view as in Figure 14 of the perturbed surface, shown together with the unperturbed surface. Note the smooth joining of the two surfaces at a line corresponding to the bounding characteristic strip of the ill–posed region.
Figure 16. A rear view of the surface recovered for $f = 2(10^6)$, corresponding to the ill–posed region of the object in Figure 1. The position of the viewer is into the page.
Figure 17. The same view as in Figure 16 of the perturbed surface, shown together with the unperturbed surface.
Figure 18. A second example of an object with an unconstrained image region, viewed from above and projected into the x–y plane.
Figure 19. The same object as in Figure 18, projected into the image plane.
Figure 20. The characteristic flow on the object considered in section 7, viewed from above and projected into the x–y plane.

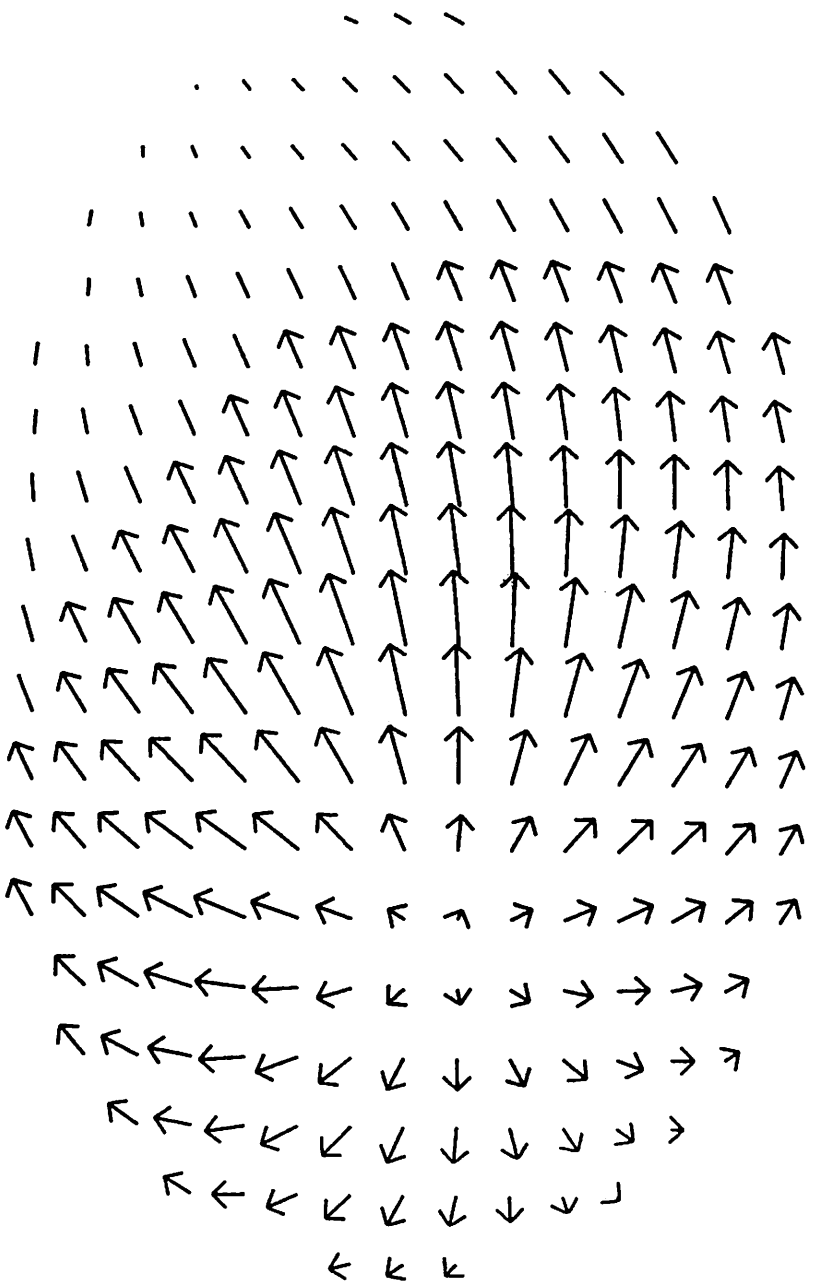

Figure 1.

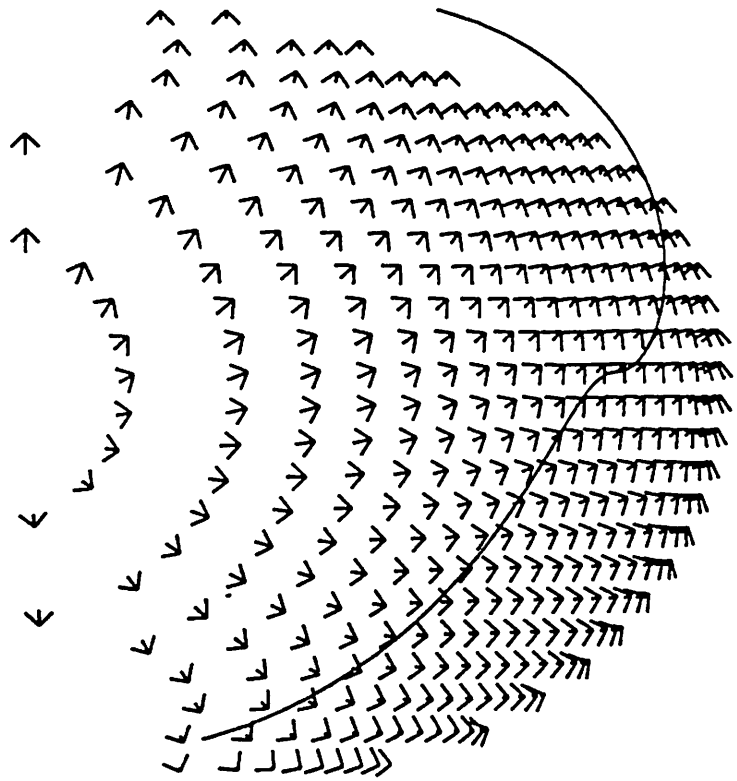

Figure 2.

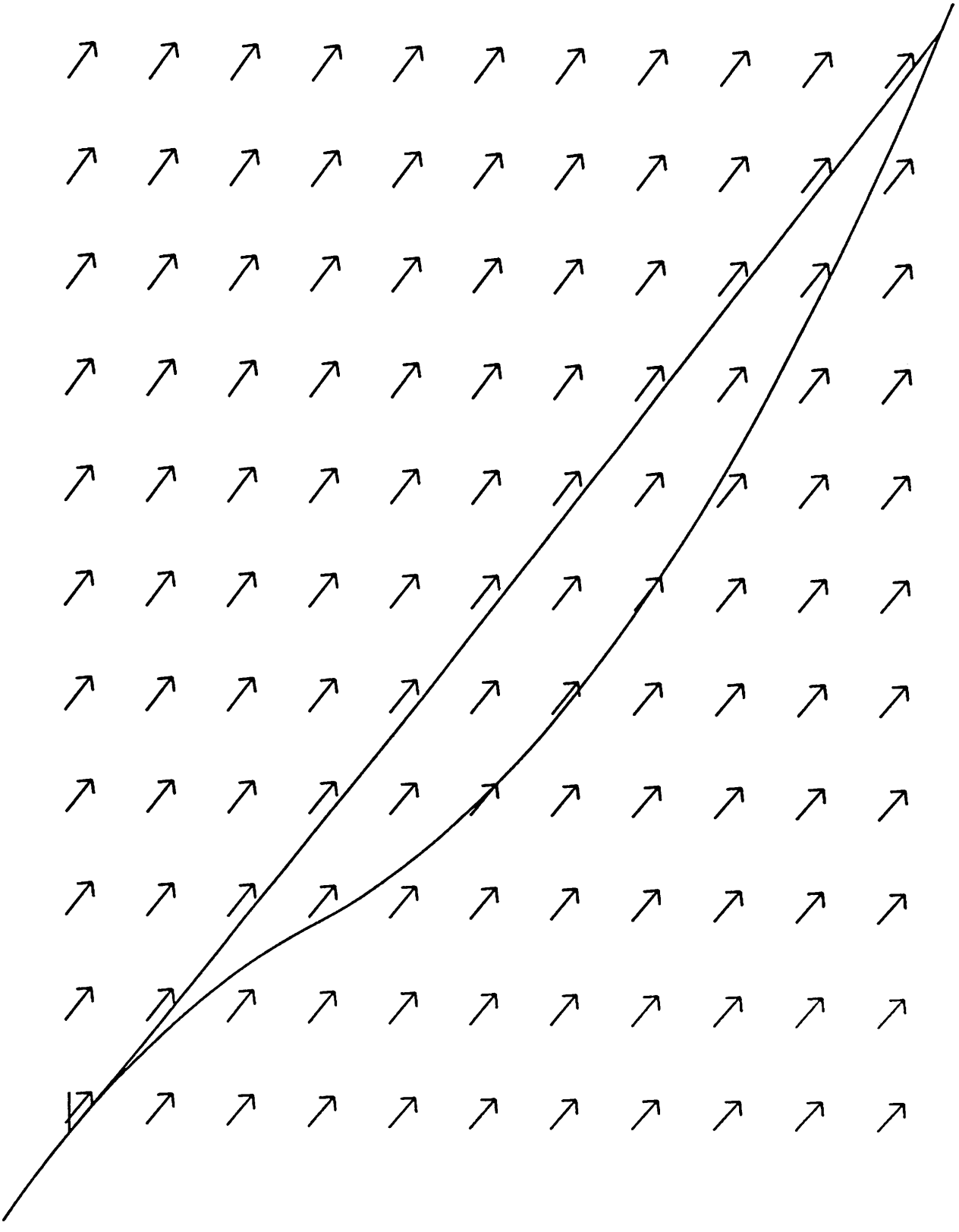

Figure 3.

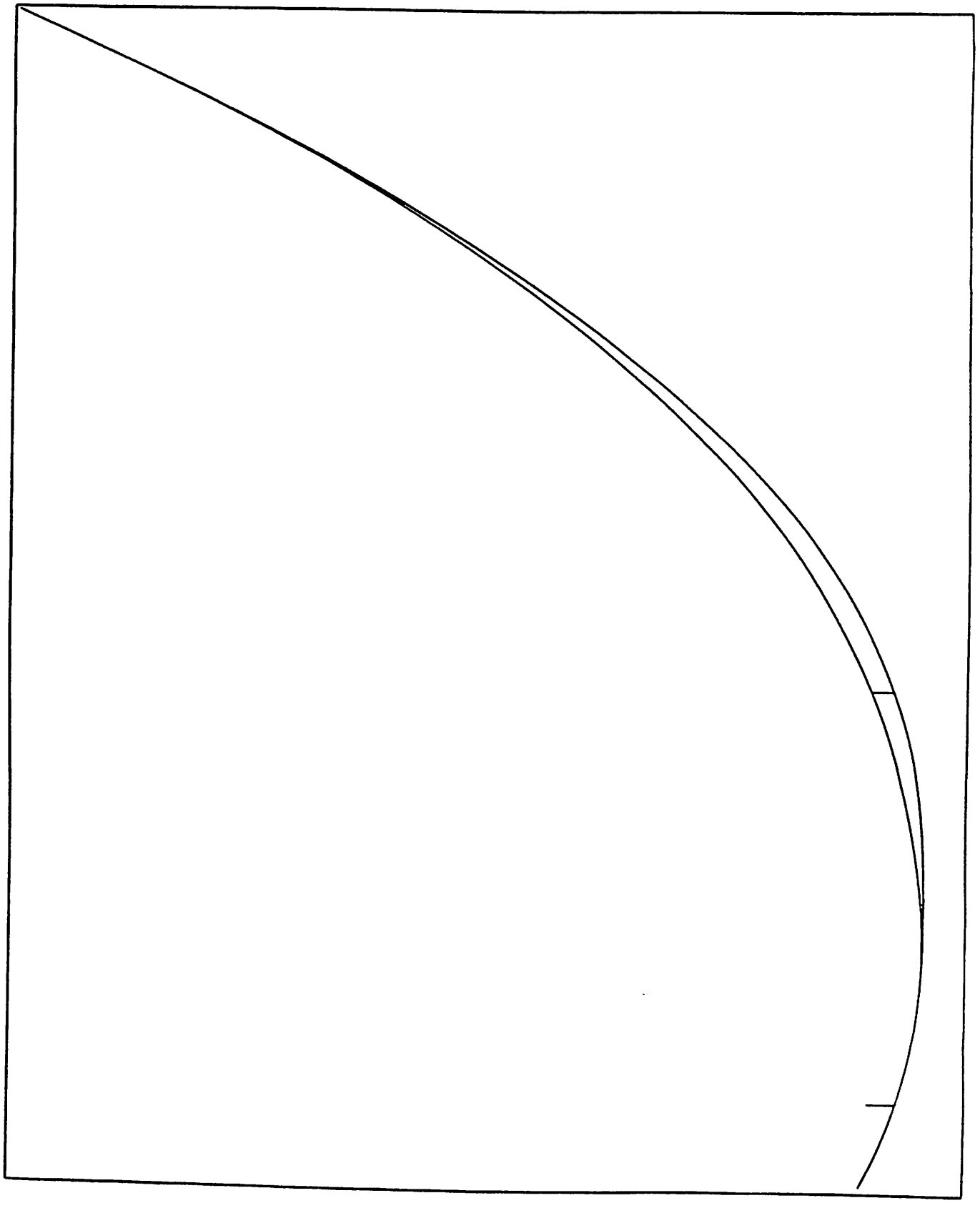

Figure 4.

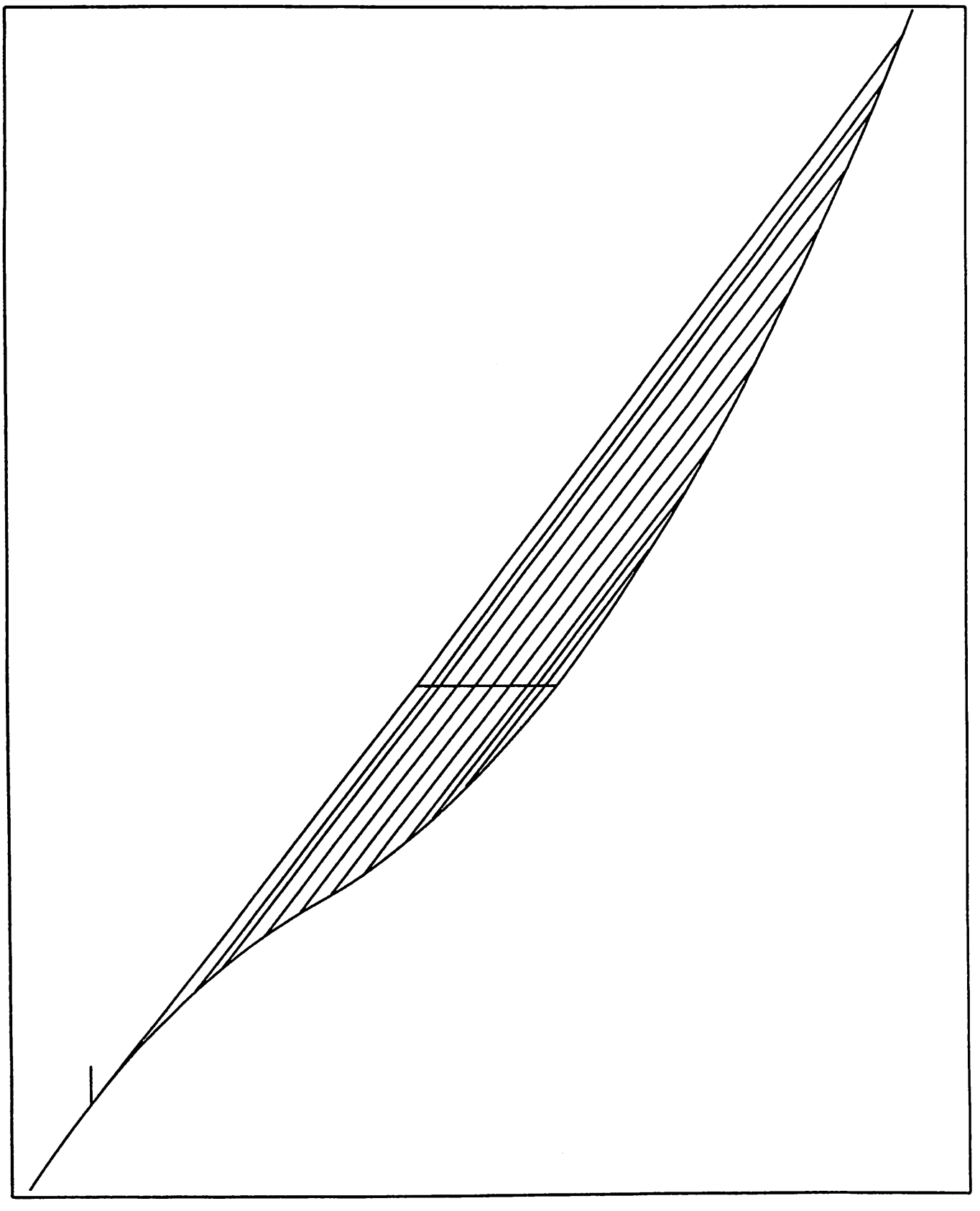

Figure 5.

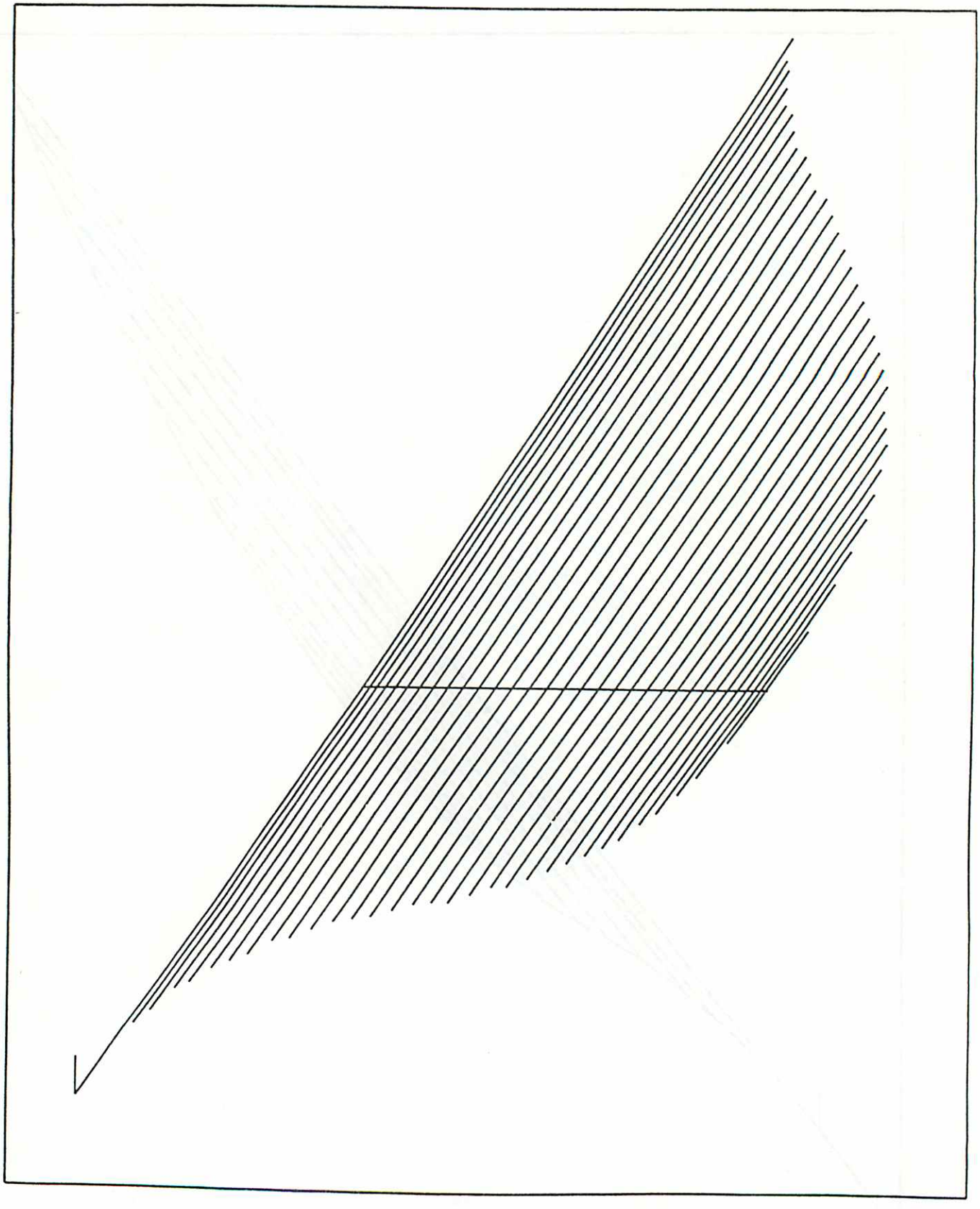

Figure 6.

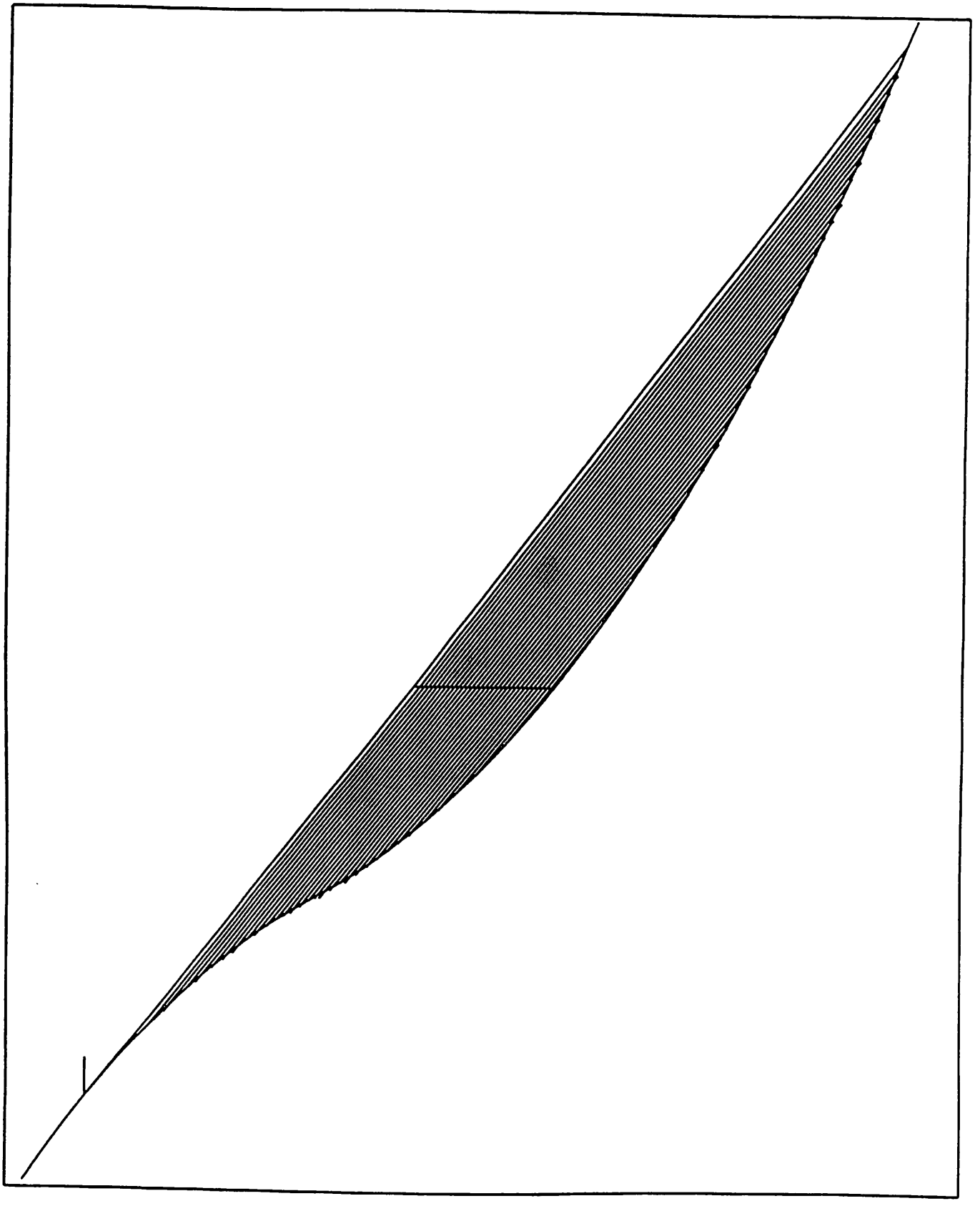

Figure 7.

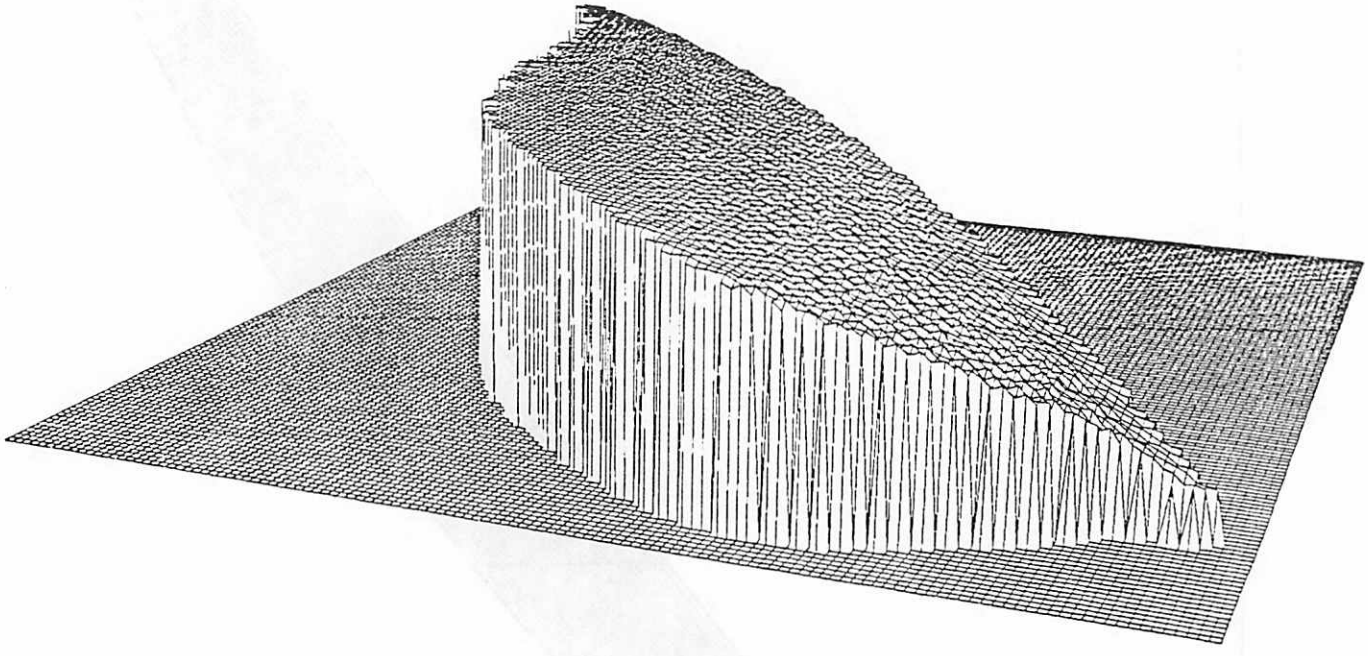

Figure 8.

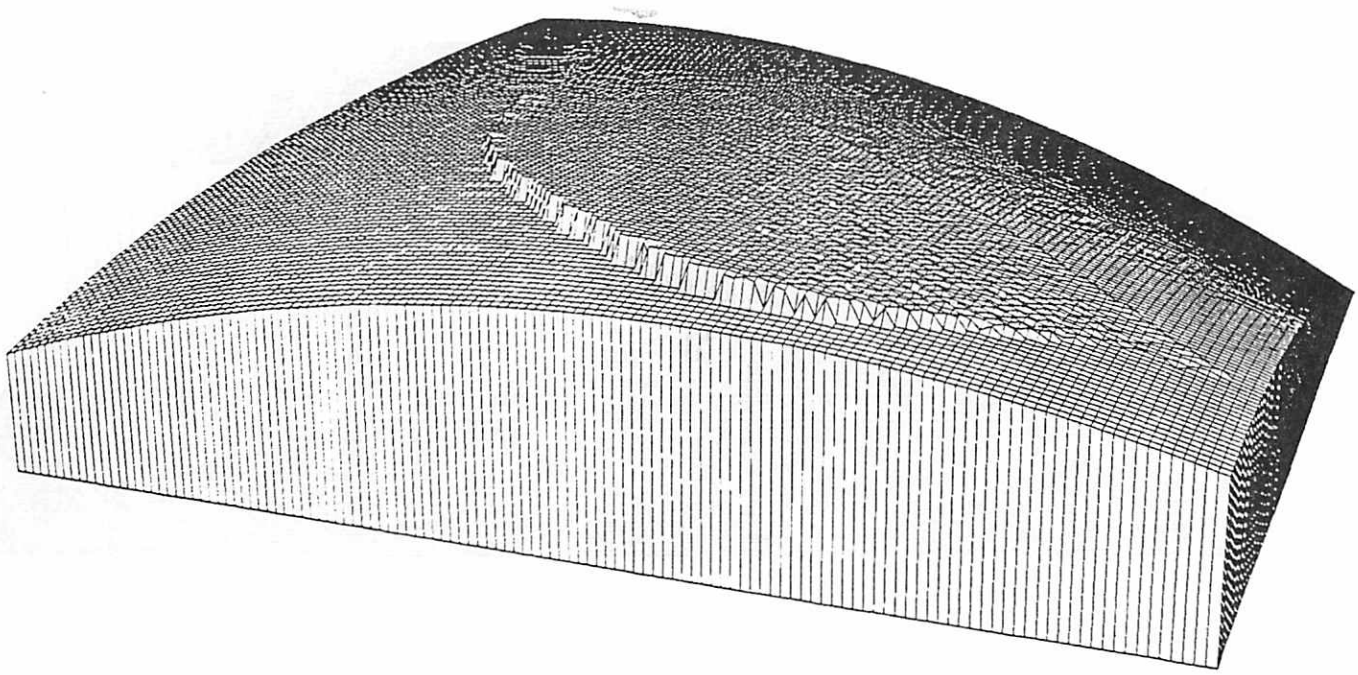

Figure 9.

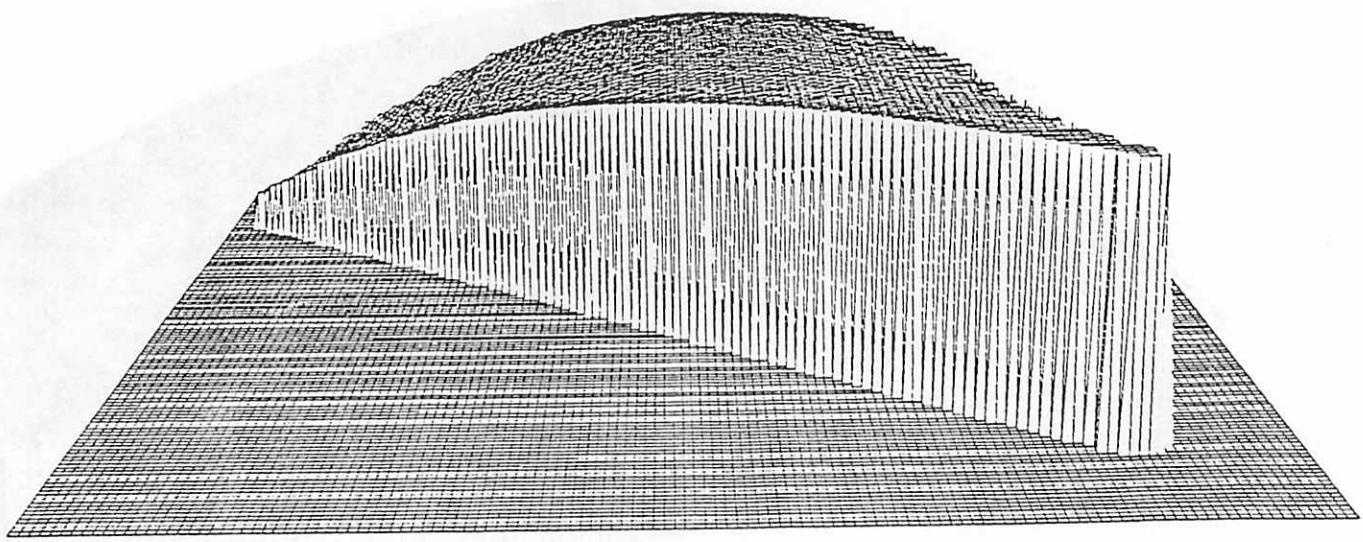

Figure 10.

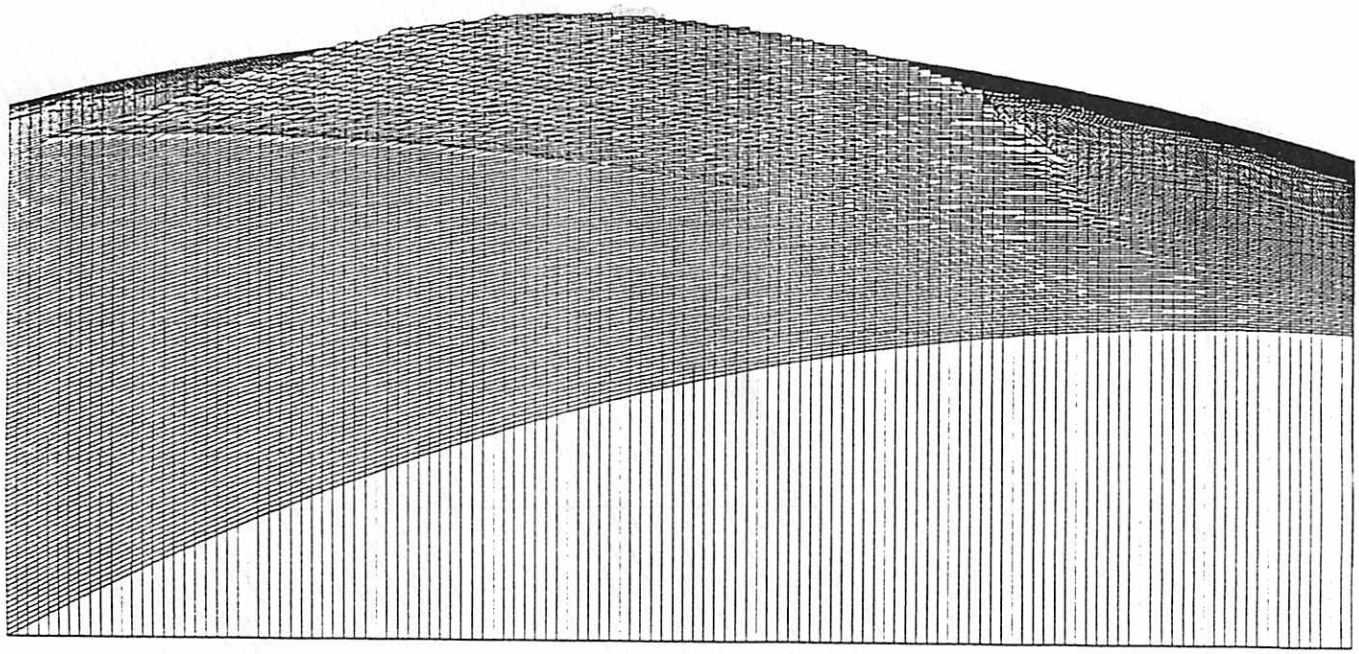

Figure 11.

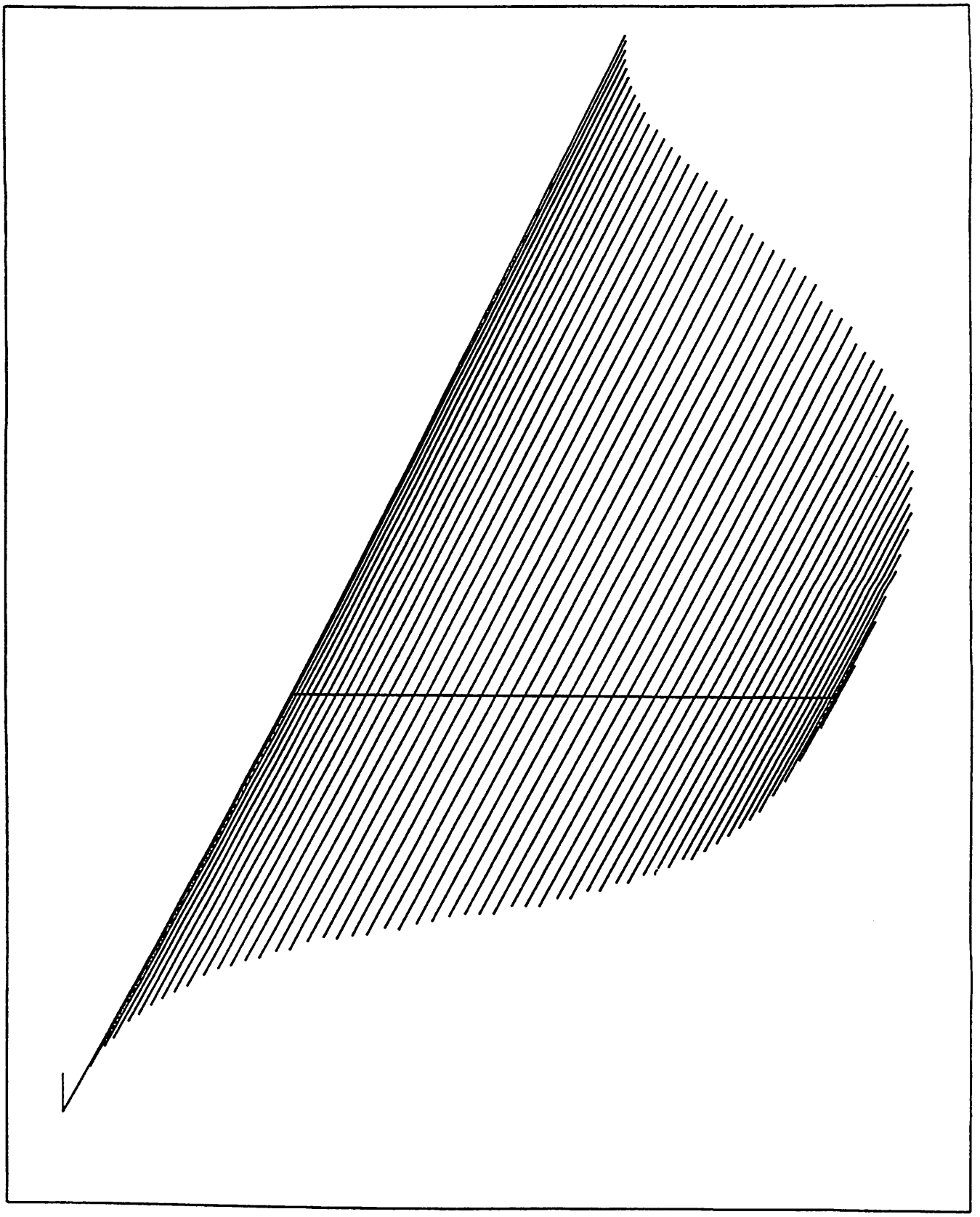

Figure 12.

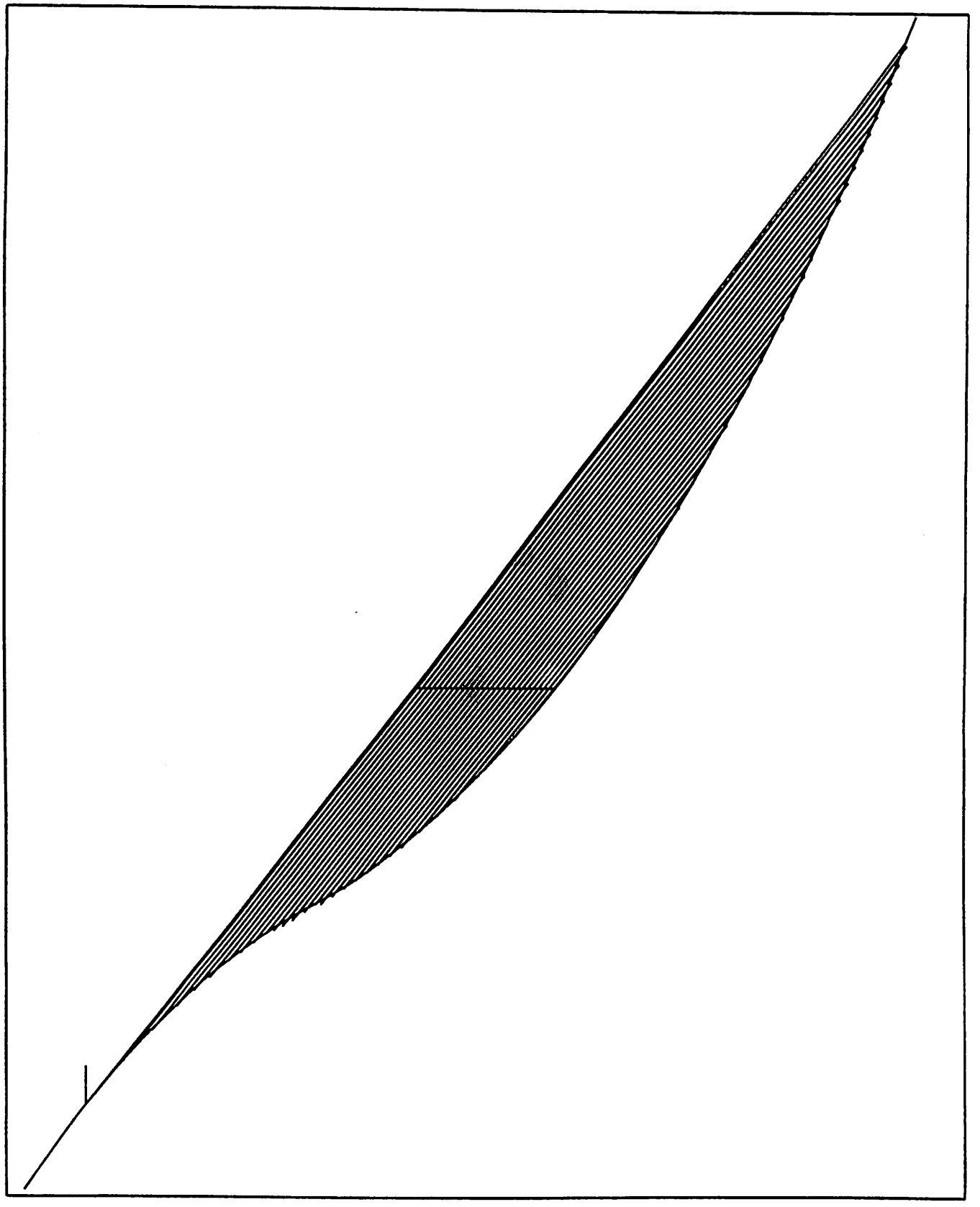

Figure 13.

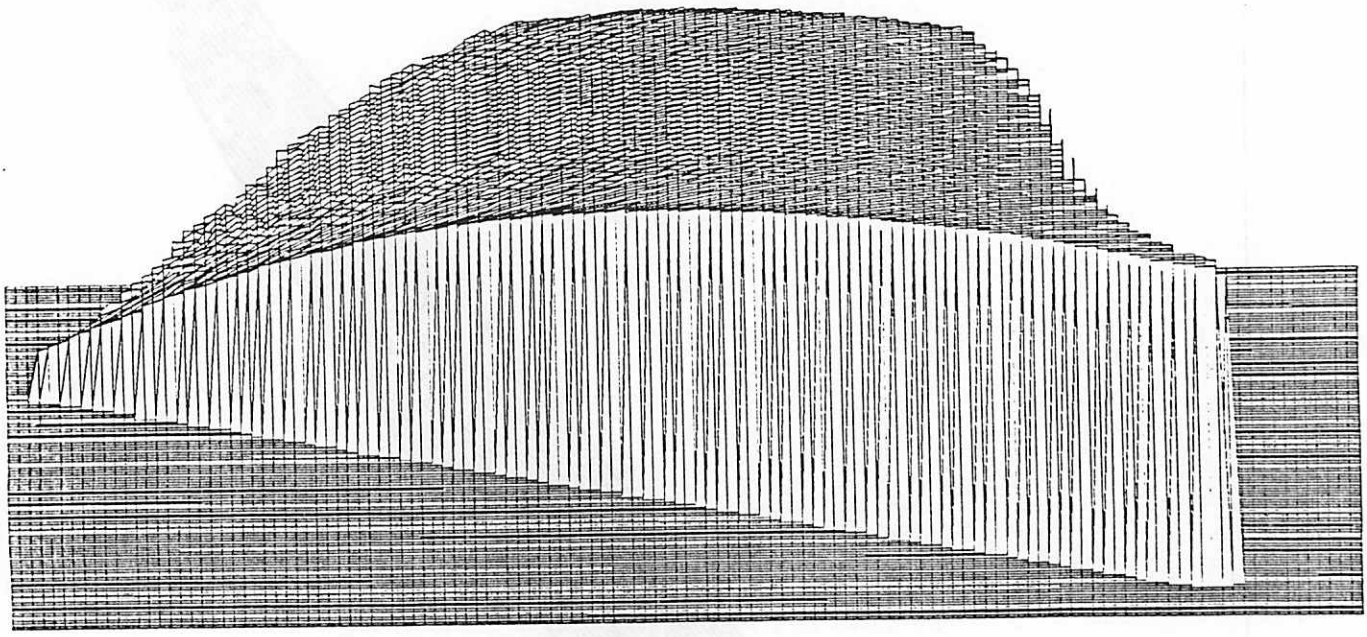

Figure 14.

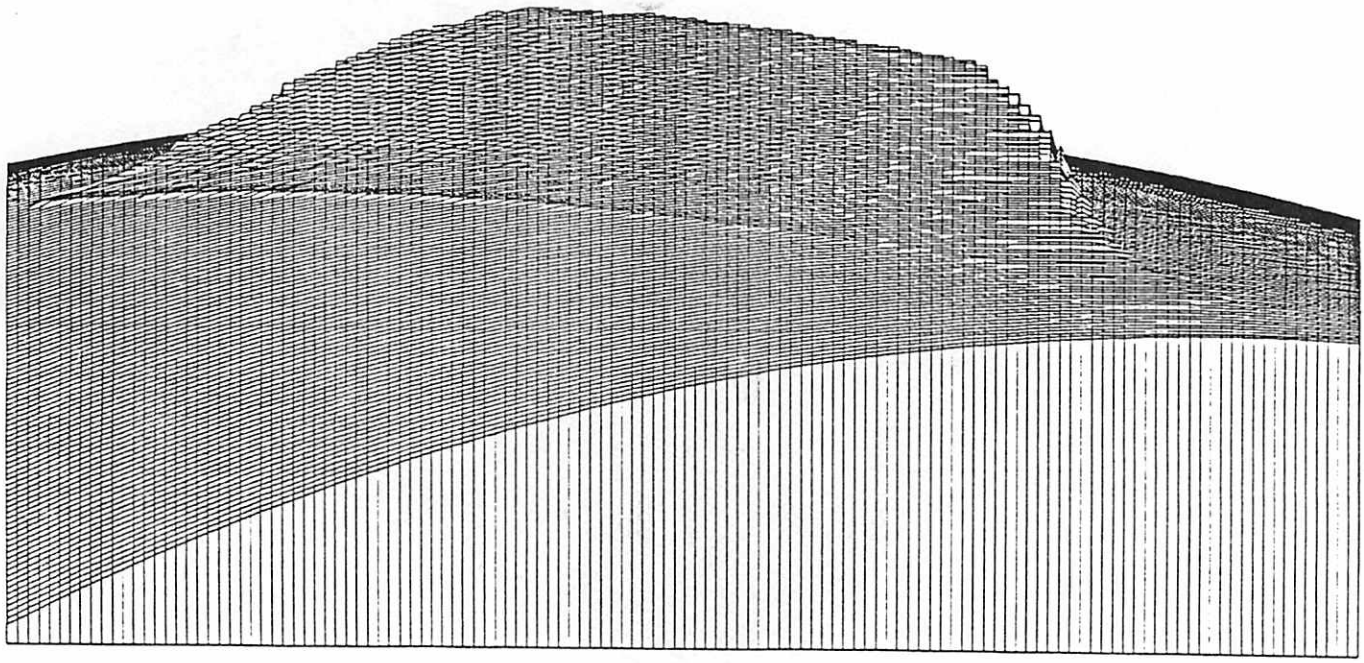

Figure 15.

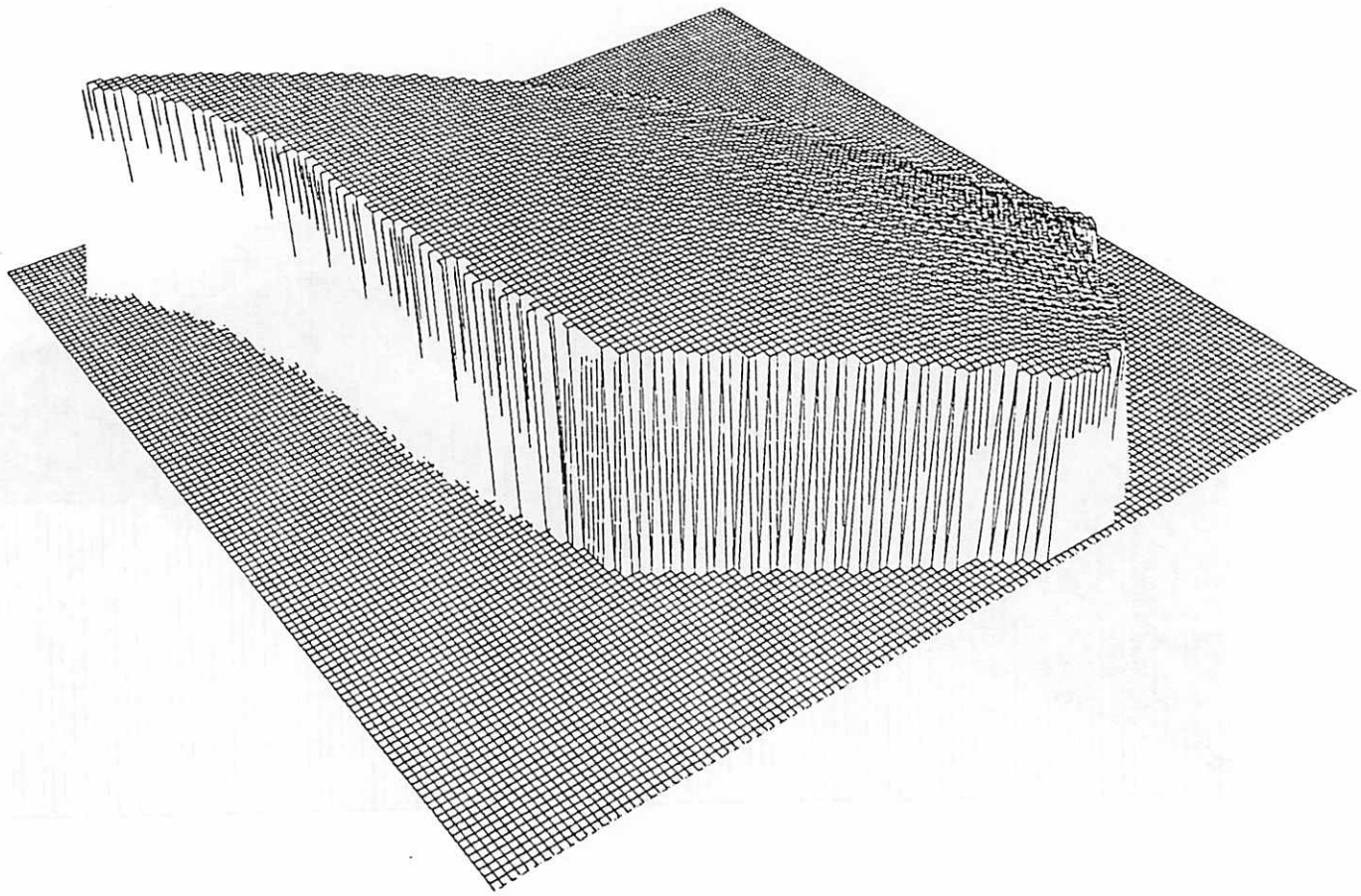

Figure 16.

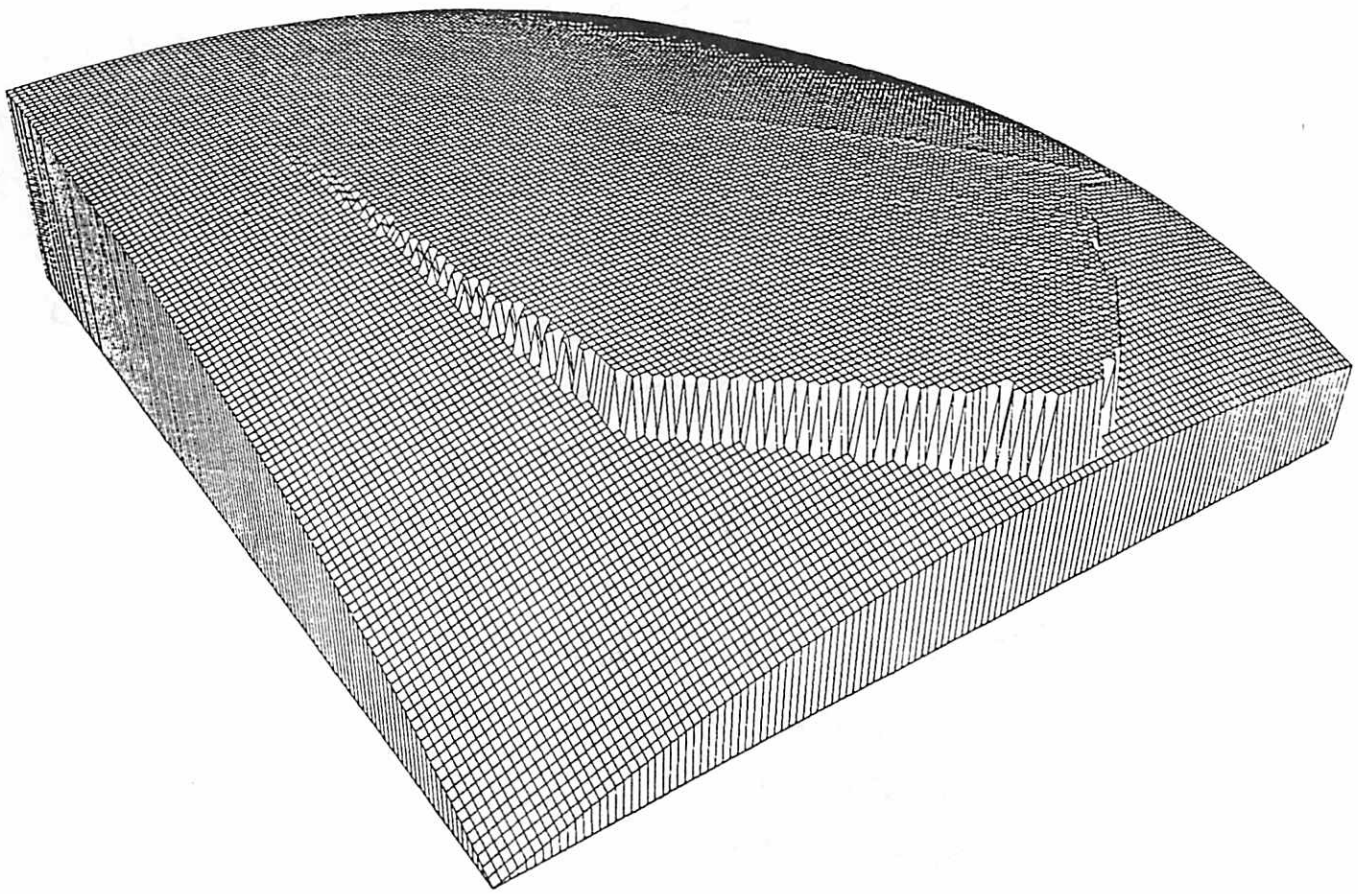

Figure 17.

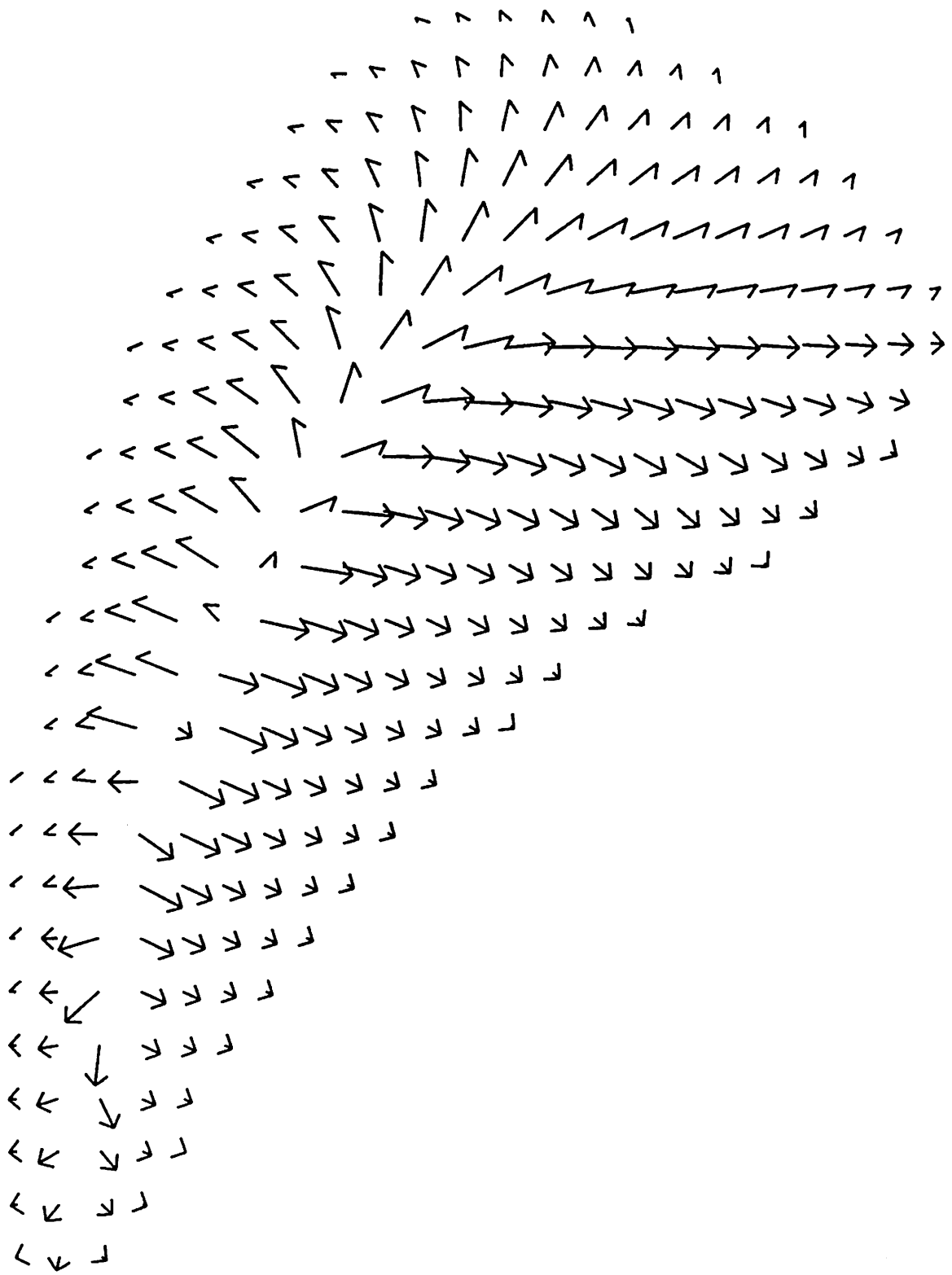

Figure 18.

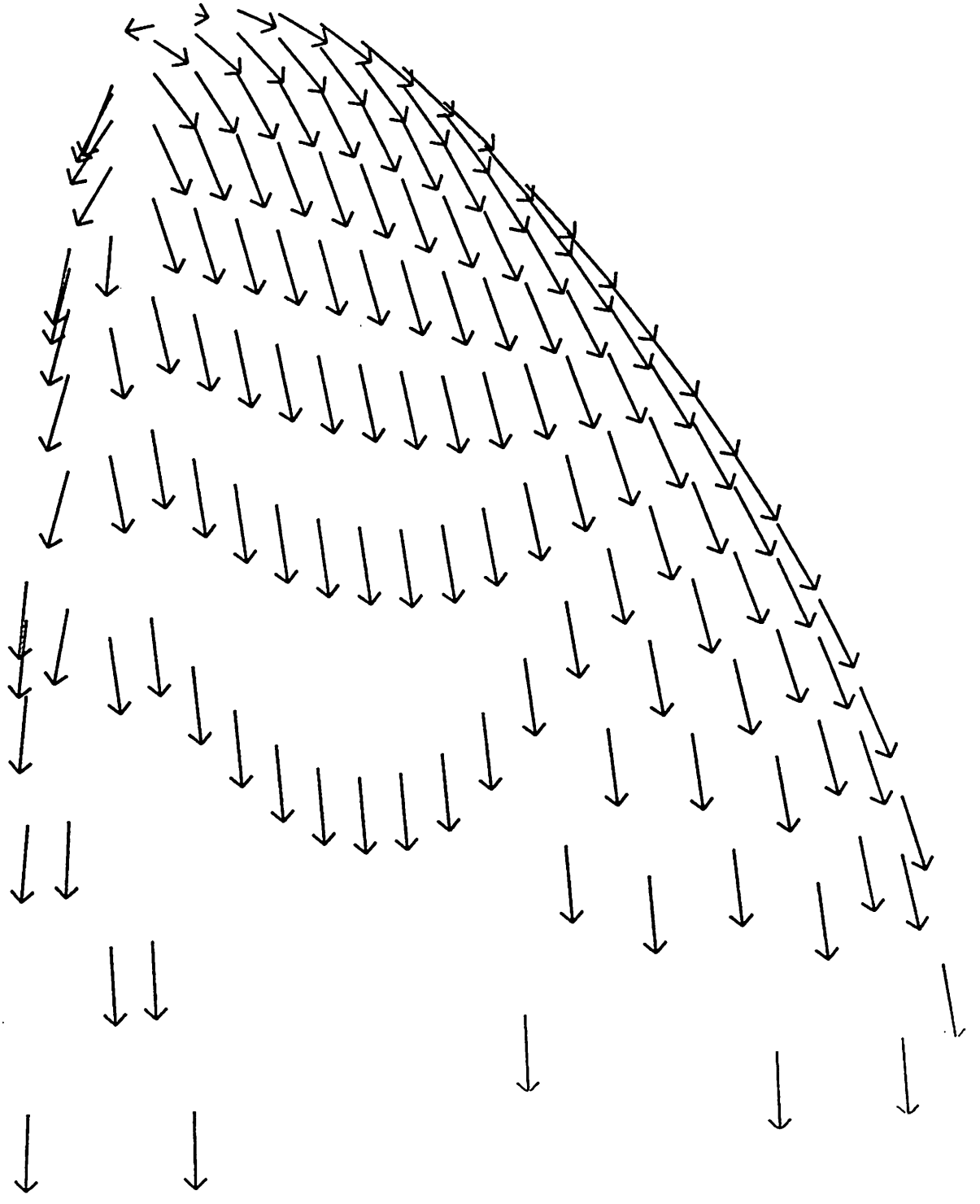

Figure 19.

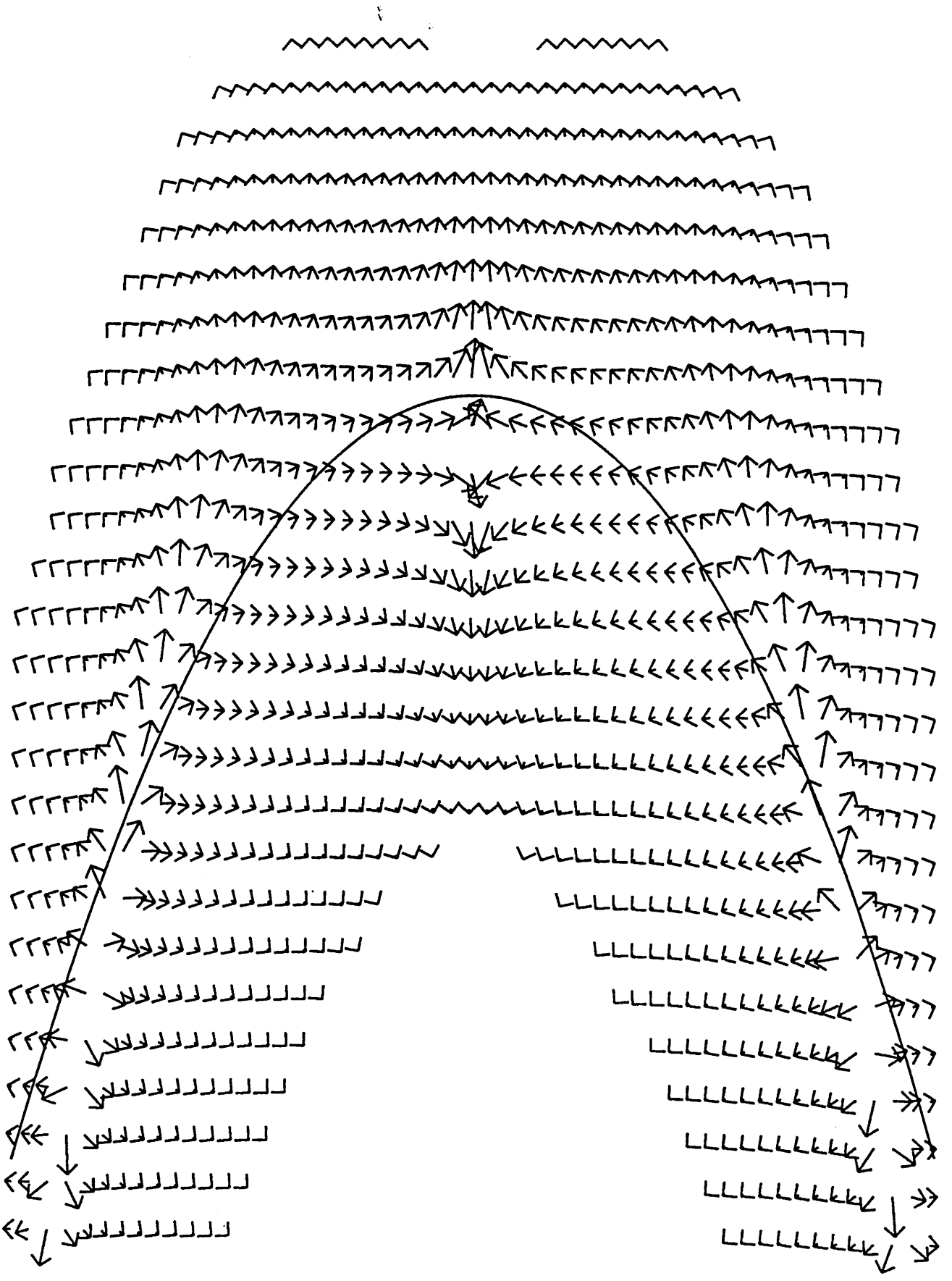

Figure 20.